Sulphur-rich functionalized calix[4]arenes for selective complexation of Hg^{2+} over Cu^{2+}, Zn^{2+} and Cd$^{2+†}$

Bachir Bensenane[ab], Zouhair Asfari[a], Carlos Platas-Iglesias[c], David Esteban-Gómez[c], Fatiha Djafri[b], Mourad Elhabiri[d] and Loïc J. Charbonnière[a]

[a] Laboratoire d'Ingénierie Moléculaire Appliquée à l'Analyse (LIMAA), IPHC – UMR 7178 – CNRS, ECPM, Bât R1N0, 25 rue Becquerel, 67087 Strasbourg Cedex 02, France

[b] Laboratoire de Chimie des Matériaux, Faculté des Sciences Exactes et Appliquées, Université d'Oran1 Ahmed Ben Bella, 31000 Oran, Algeria

[c] Universidade da Coruña, Centro de Investigacións Científicas Avanzadas (CICA) and Departamento de Química Fundamental, Facultade de Ciencias, 15071, A Coruña, Galicia, Spain

[d] Laboratoire de Chimie Bioorganique et Médicinale, UMR 7509 – CNRS, ECPM, 25, rue Becquerel, 67087 Strasbourg Cedex 02, France

How to cite:

Abstract

The syntheses of two new ligands based on a calix[4]arene scaffold in the cone conformation functionalized on the phenolic positions 1 and 3 by diethylthiophosphonates (**L1**) or tetra(tri)thioethyleneglycol (**L2**) crowns are described. Together with ligand **L3**, the parent calix[4]arene substituted by a penta(tetra)thioethyleneglycol crown, the spectroscopic properties of the ligands were determined by means of UV-Vis absorption spectroscopy and steady-state and time-resolved fluorescence spectroscopy, showing that the ligands display modest but non-negligible intrinsic fluorescence properties (ϕ_{fluo} = 0.023; 0.026 and 0.029 for **L1**, **L2** and **L3** in CH$_2$Cl$_2$, respectively). The X-ray crystal structures of ligand **L1**, and of its synthetic precursor were determined and analyzed for their capacity to accommodate the incoming cationic species. The ligands were further investigated for their complexation properties of divalent cations such as Cu^{2+}, Zn^{2+}, Hg^{2+} and Cd^{2+} (under their nitrate salts) in 1 : 1 CH$_3$CN/CH$_2$Cl$_2$ solutions (I = 0.01 M Et$_4$NNO$_3$, T = 25.0(2) °C), in which the additions of cations were monitored by absorption and steady-state fluorescence spectrophotometries. The stoichiometries of the corresponding complexes were assessed by ESI-MS, while insights into the structures of the complexes in solution were obtained with density functional theory (DFT) calculations. The influence of the sulphur and phenol coordinating moieties was addressed to show that the thiocrown compounds **L2** and **L3** displayed a marked affinity towards the soft mercuric cation (Δlog $K \geq 2$), with no particular size selectivity effect, whereas ligand **L1** can accommodate both the thio and phenol units to coordinate with Cu(II). Altogether, these results point to the use of **L3** as a selective fluoroionophore for detection of Hg^{2+}.

Keywords: calix[4]arenes; DFT calculations; heavy-metal complexes; stability constants; thiocrown ethers

Introduction

Since their first characterization,[1] calixarenes have received considerable attention as a result of their easy synthetic access, size varying macrocyclic structures, conformational diversity and large chemical versatility.[2] Their upper or lower rim functionalization combined with the macrocyclic scaffold has attracted much interest for complexation of cationic, neutral and anionic species,[3] selective complexation and extraction,[4] bioorganic applications[5] or luminescent devices.[6] Owing to their large polyaromatic structures, calixarenes are basically hydrophobic molecules, unless they are substituted by water solubilizing groups such as amino-acids,[7] or sulfonate functions.[8] On the other hand, when adequately functionalised by complexing arms, they might provide excellent preorganised binding moieties for biphasic extraction and purification of traces of heavy metals such as mercury (Hg^{2+}) or cadmium (Cd^{2+})[9] contained in aqueous phases. Due to their soft (Hg^{2+}) or borderline (Cd^{2+}) Lewis acid character, calixarenes containing soft base binding moieties like thioethers and/or dialkylthiophosphate have been the focus of interest. For instance, *p-tert*-butyl-thio- and *p-tert*-butyl-calix[4]arenes substituted by diethylthiophosphate ester groups (-P(S)(OEt)$_2$) have been reported and their heavy cation binding properties (Hg^{2+}, Ag^{2+}, Cd^2, *etc.*) have been thoroughly described.[10] *p-tert*-Butyl-thiocalix[4]arenes comprising cyclic or linear (O,S,N) ligating and/or π-coordinating groups on the lower rim have been found to be selective ionophores for Ag^+.[11] It is also noteworthy that calix[4]resorcinols substituted with thiophosphoryl fragments, that are resistant to hydrolysis and electrochemical oxidation, displayed high complexing ability toward nickel cations.[12]

Following our ongoing interest in the recovery of heavy metals such as mercury and cadmium present in some waste waters,[9c,13] we have focused our attention in this present work to the use of sulphur functionalized calixarene ligands L1 to L3 (Scheme 1) as potential fluoroionophores.
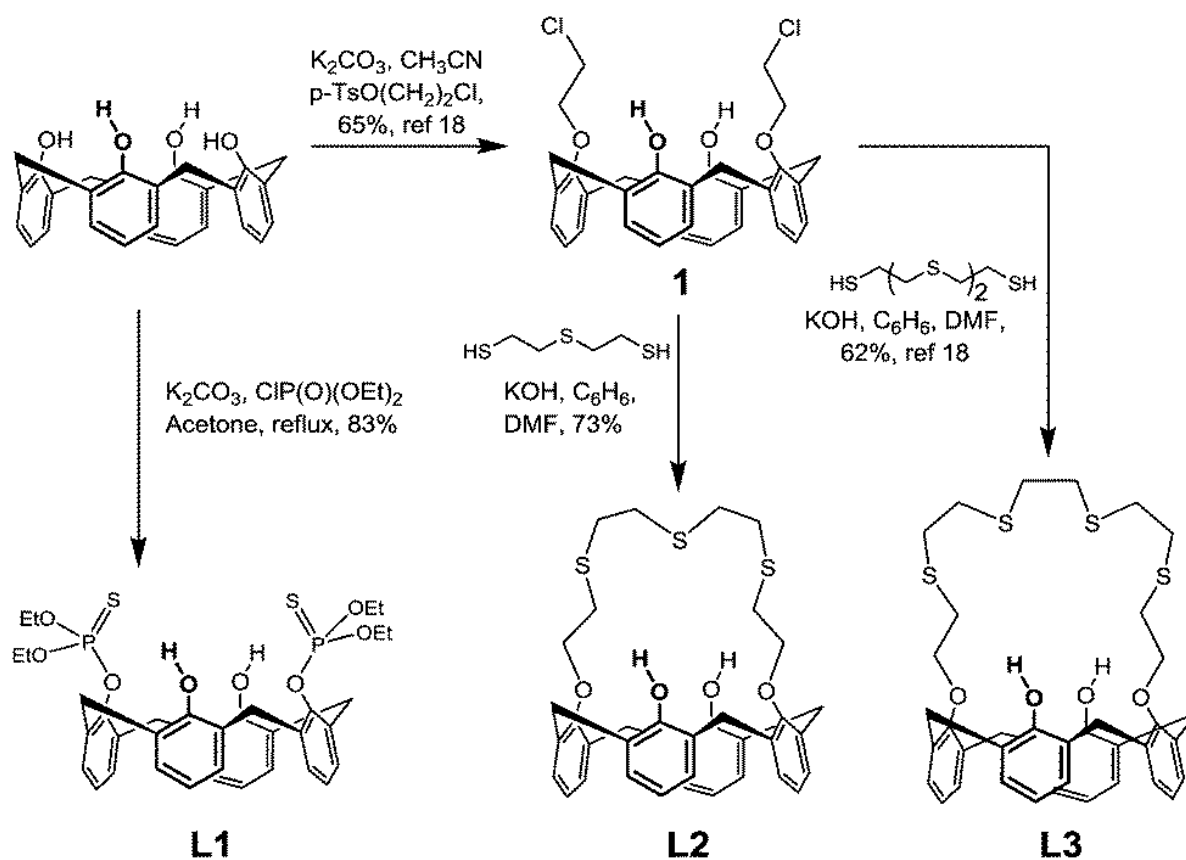
Scheme 1. Structures of ligands **L1** to **L3** and the synthetic protocols used for their preparation.

Although numerous reports deal with the use of calixarenes as fluoroionophores for cation sensing,[14] these studies mainly focus on macrocycles that have been derivatised with organic fluorescent reporters and only a few studies have been specifically focused on the intrinsic fluorescence properties of calixarenes, apart from particular ones obtained from polyphenyl moieties.[15] Similarly, ON–OFF or OFF–ON fluorescent responses of azathiocrown ethers for Hg^{2+} detection were achieved by introducing organic fluorophores (dansyl[16] or BODIPY[17]). In the present study, the spectrophotometric (absorption and fluorescence emission) properties of the ligands **L1** to **L3** are discussed and are advantageously used to monitor and quantify the coordination of selected divalent heavy metal ions such as Hg^{2+}, Cd^{2+}, Cu^{2+} and Zn^{2+}.

Results and discussion

Synthesis of the ligands

Ligand **L1** was obtained in 83% yield by a selective substitution of calix[4]arene on the 1 and 3 phenolic rings using diethylthiochlorophosphate in acetone and K_2CO_3 as a base (Scheme 1). **L1** closely resembles a *p-tert*-butyl-calix[4]arene analogue for which a much lower yield was obtained (26%, $ClP(S)(OEt)_2$, K_2CO_3, CH_3CN).[10] Despite the poor quality of the refinement, the X-ray crystal structure of ligand **L1** and crystal data are presented in the ESI (Fig. S1 and cif file†). It is noteworthy that the solid state structure of the *p-tert*-butyl-calix[4]arene analogue of **L1** was reported as well.[10] Ligand **L2** was obtained in a similar manner to **L3**[18] in two synthetic steps by first introducing 2-chloroethoxyl groups on the 1 and 3 phenolic rings of the calix[4]arene, to obtain intermediate **1**, followed by cyclization of the crown using 3-thio-1,5-dithiopentane (**L2**) or 3,6-dithio-1,8-dithiooctane (**L3**) in the presence of KOH in a benzene/DMF (2/1) mixture. The cyclization was achieved in 73% and 62% yields for **L2** and **L3** respectively. A *p-tert*-butyl analogue of **L2** has recently been described in the literature using a similar synthetic protocol,[19] as well as an analogue based on a calix[4]-bis-crown with a 1,3-alternate conformation.[20] Closely related systems such as thiocalix[4](O,S,N crown-5)ethers were also described.[11]

All calixarenes were isolated in their cone conformation, as evidenced by the C_{2v} symmetry observed in their ^{1}H- and ^{13}C-NMR spectra, and by the presence of the characteristic AB spin system of the methylene bridges joining the phenolic units.

Slow crystallization of a solution of compound **1** in CH_2Cl_2/MeOH afforded crystals suitable for X-ray diffraction analysis. The solid state structure of **1** is presented in Fig. 1 (CCDC 1476805).

As anticipated by ^{1}H-NMR measurements, the calixarene scaffold displayed the expected cone conformation, in which the H atoms of the nonalkylated phenol rings are engaged in weak H bonding interactions with the neighbouring O atoms of the phenolic ethers ($d_{H–O}$ = 1.914 and 1.984 Å, angles between O_{phenol}, H_{phenol} and O_{ether} = 157.7 and 151.0°). A second feature arising from the structure is the strong influence of the chloroethyl groups on the cone conformation. The presence of these groups forces the substituted phenol rings to flatten along the main axis (Fig. 1, left). This is evidenced by the inclination angle δ,[21] defined as the angle between the planes containing an aromatic ring and the best plane containing the methylene bridges. Whereas the C_4 symmetrically substituted calixarenes display typical inclination of 113–115°,[22] the inclination of the substituted rings of **1** are both of 110°, and those of the non-substituted phenols are of 144°, pointing to a flattened cone conformation. Finally, one can also notice that the compound is fairly well pre-organized for the closing of the crown ether chain, explaining the relatively good chemical yields obtained in the cyclization steps of **L2** (73%) and **L3** (62%).

Slow concentration of a $CDCl_3$ solution of **L2** afforded crystals suitable for X-ray diffraction analysis. Fig. 2 displays the solid state structure of **L2** (CCDC 1476806).
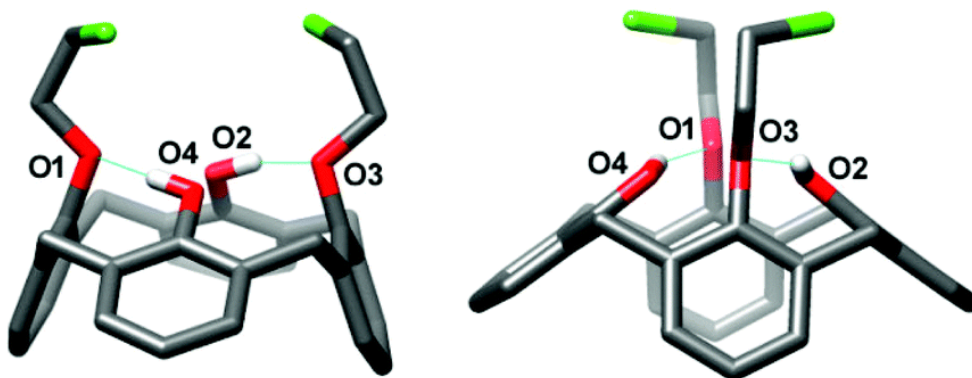
Fig. 1. X-ray crystal structure of compound **1** (H atoms are omitted for the sake of clarity, except those involved in H-bonding interactions, C = grey; O = red; H = white; Cl = green).
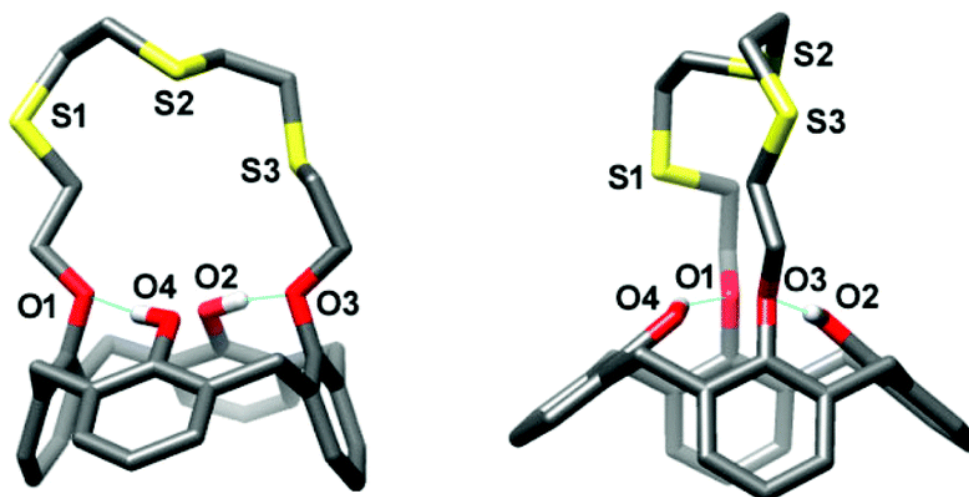

Fig. 2. X-ray crystal structure of **L2** (hydrogen atoms are omitted for the sake of clarity, except for the phenolic protons involved in hydrogen bonds drawn as dashed lines. C = grey; O = red; H = white; S = yellow).

As for **1**, the solid state structure of **L2** confirms the cone structure previously assumed on the basis of the ^{1}H NMR data. The hydrogen atoms of the unsubstituted phenol rings are also weakly bonded to the neighbouring oxygen atoms of the adjacent substituted phenol rings (d_{H-O} = 1.934 and 1.979 Å, angles between O_{phenol}, H_{phenol} and O_{ether} = 165° and 154°). The impact of the closing of the thiocrown ether chain was rather poor; the inclination angle δ is almost unchanged for the non-substituted phenol rings (142 and 143° for **L2**), while those of the substituted phenol rings are slightly increased to 113 and 115° (110° for **1**) upon ring closure. The crystal structure of **L1** is given in Fig. S1 and S2 (ESI†).

Spectroscopic properties of the ligands

The UV-Vis absorption spectra of ligands **L1**, **L2** and **L3** in CH$_3$CN/CH$_2$Cl$_2$ are presented in Fig. 3, together with their respective fluorescence spectra. The main photophysical characteristics of the ligands are summarised in Table 1. At first glance, one can notice the close similarity of the absorption spectra of **L2** and **L3**, showing that the size of the thiocrown ether does not influence the spectrophotometric properties of the calix[4]arene scaffold.
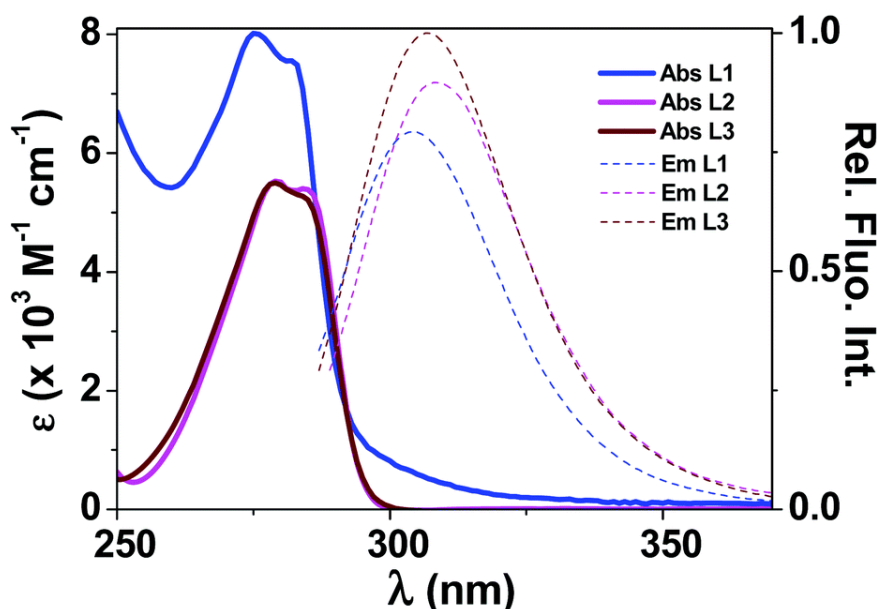
Fig. 3. UV-Vis absorption electronic (full lines) and fluorescence (dashed lines) spectra of ligands **L1** (blue, λ_{exc} = 287 nm), **L2** (magenta, λ_{exc} = 287 nm) and **L3** (brown, λ_{exc} = 287 nm) in a 1/1 (v/v) CH_3CN/CH_2Cl_2 mixture at 25.0(2) °C. Emission spectra normalized with respect to their quantum yields (Table 1).

Table 1. Main spectroscopic properties of ligands L1, L2 and L3[a]

Ligand	λ^{abs}_{max} (ε) [nm ($M^{-1}cm^{-1}$)]	λ^{em}_{max}(nm)	λ^{abs}_{max} (ε) [nm ($M^{-1}cm^{-1}$)]	λ^{em}_{max}(nm)	ϕ_{fluo}(%)	τ(ns)	k_r[b]($\times10^{-7}s^{-1}$)	k_{nr}[b]($\times10^{-7}s^{-1}$)
	CH_3CN/CH_2Cl_2(1/1)		CH_2Cl_2					
L1	275 (8010)	304	276 (6980)	304	2.3	1.2	1.9	81
	282 (7550)		282 (6640)					
L2	279 (5530)	309	279 (10 480)	307	2.9	1.4	2.0	67
	284 (5400)		284 (9950)					
L3	279 (5500)	307	278 (9120)	307	2.6	1.5	1.7	63
	284 (5280)		284 (8490)					

[a] T = 25.0(2) °C. Estimated errors in λ, ε and ϕ_{fluo} are ±1 nm, ±5% and ±10%, respectively. [b] Defined by $k_r = \phi_{fluo}/\tau$ and $k_{nr} = (1 - \phi_{fluo})/\tau$; ref. 23).

In dichloromethane, the UV-Vis absorption spectra are dominated by intense $\pi \rightarrow \pi^*$ transitions centred on the phenol rings of the calix[4]arene backbone. Interestingly, the absorption is strongly solvent-dependent, as the change from CH_2Cl_2 to a mixed solvent made of CH_2Cl_2 and CH_3CN (50/50 v/v) led to a strong increase of the absorption coefficients, with almost no spectral shift of the absorption bands. The introduction of a more polar solvent (required for the dissolution of metal nitrate salts) likely plays an important role in the hydrogen bonding interactions, with a concomitant hyperchromic effect, especially for **L2** and **L3**. It is noteworthy that the absorption spectra of the ligands display two distinct absorption bands at their maximum of absorption, a feature that is typical of calixarenes, whatever their ring size.[24]

Upon excitation into the UV-Vis absorption bands, all three calixarenes displayed an emission band with the maximum lying at about 304–309 nm. On account of the nanosecond lifetimes of the emitted signals, these emission bands can be ascribed to $^1\pi\pi^*$ emission. The corresponding luminescence quantum yields are rather

small, but however not negligible, amounting to more than *ca.* 2–3%, and they are only poorly dependent on the substitution pattern of the calixarene. From the analysis of the radiative and non-radiative decay of the compounds, it clearly appears that this weak fluorescence emission is the result of efficient non-radiative processes that may be related in part to a potential redox activity of the phenol rings in the excited state.

Characterisation of the metal complexes

We investigated the ability of ligands **L1–L3** to bind divalent heavy metal cations such as Hg^{2+}, Cd^{2+}, Cu^{2+} and Zn^{2+}. The stoichiometries of the metal complexes formed with ligands **L1–L3** were first assessed by electrospray ionisation mass spectrometry (ESI-MS) in the positive mode. The ESI-MS mass spectra were recorded for CH_3CN/CH_3OH (1/1 v/v) solutions containing equimolar concentrations of metal cations (Hg^{2+}, Cd^{2+}, Cu^{2+}) and the ligands (Fig. 4). For Zn^{2+}, the $[M]_0/[L]_0$ ratio was varied up to 6 equivalents (see Fig. S23–S34, ESI,† for the other systems).

Regardless of the nature of the ligand and the metal ion, only monometallic monochelates were systematically detected, which strongly suggests that the ligands considered herein display suitable denticity and pre-organization to fulfil the stereochemical requirements of the divalent heavy metal ions. The characteristic coordination number and stereochemical arrangement of Hg^{2+} complexes are two-coordinate (linear) and four-coordinate (tetrahedral). Octahedral coordination is less common and only a few three- and five-coordinate complexes are known. For Zn^{2+} and Cd^{2+} (d^{10} configuration, no ligand field stabilization), the stereochemistry of their metal complexes is determined by the considerations of size or electrostatic interactions (CN 4 to 6 commonly observed).[25] The ionization of the cupric complexes was systematically obtained by reduction of the metallic center, while deprotonation (likely through deprotonation of the phenolic units) of the ligands led to positively monocharged species with the other metal cations. The mass of the pseudo-molecular ions of the different species observed are collected in Table 2; they are in excellent agreement with the simulated masses.

Table 2. Intensity maxima of the ESI-MS pseudo-molecular ions of the metallic complexes formed with ligands **L1–L3**[a]

L1	m/zexp.	m/zcalc.	L2	m/zexp.	m/zcalc.	L3	m/zexp.	m/zcalc.
$[L1 + H^+]^+$	729.40	729.19	$[L2 + Na^+]^+$	653.35	653.18	$[L3 + Na^+]^+$	713.35	713.18
$[L1 + Cu^+]^+$	791.30	791.12	$[L2 + Cu^+]^+$	693.30	693.13	$[L3 + Cu^+]^+$	753.30	753.14
$[L1 + Hg^{2+} - H^+]^+$	929.30	929.14	$[L2 + Hg^{2+} - H^+]^+$	831.35	831.16	$[L3 + Hg^{2+} - H^+]^+$	891.35	891.16
$[L1 + Cd^{2+} - H^+]^+$	841.25	841.08	$[L2 + Cd^{2+} - H^+]^+$	743.30	743.09	$[L3 + Cd^{2+} - H^+]^+$	803.30	803.09
$[L1 + Zn^{2+} - H^+]^+$	791.25	791.10	$[L2 + Zn^{2+} - H^+]^+$	693.25	693.11	$[L3 + Zn^{2+} - H^+]^+$	753.35	753.12

[a] Solvent: CH_3CN/CH_3OH (1/1 v/v). Positive mode; skimmer voltage ranges from 150 V to 200 V. $[L]_0 \sim 5 \times 10^{-5}$ M. $[M^{2+}]_0/[L]_0 \sim 1$ for Hg^{2+}, Cu^{2+} and Cd^{2+} and $[M^{2+}]_0/[L]_0 \sim 1$ to 6 for Zn^{2+}.

Spectrophotometric titrations of L1–L3 with Hg^{2+}, Cd^{2+}, Cu^{2+} and Zn^{2+}

To further characterise and quantify the interactions between the thiocrown ether or thiophosphate binding sites and the divalent metal cations, UV-Vis absorption spectrophotometric titrations of **L1**, **L2** and **L3** were carried out by additions of increasing volumes of solutions of the metal nitrate salts in a mixed solvent system composed of acetonitrile and dichloromethane (1/1 v/v). Fig. 5 and 6 exemplify the absorption spectral variations obtained with Hg^{2+}/**L2** and Cu^{2+}/**L3**, respectively (see Fig. S3–S22, ESI,† for the other titrations).
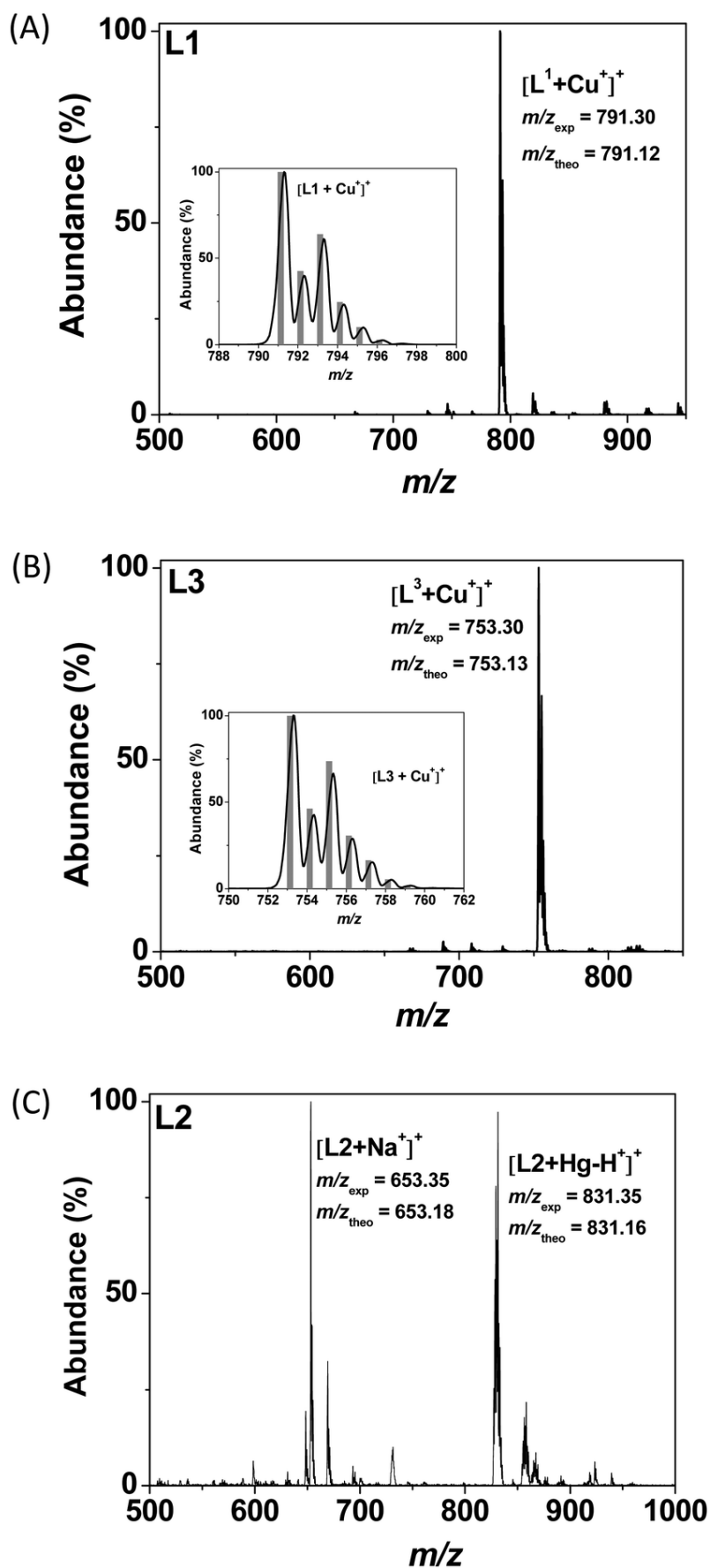
Fig. 4. ESI mass spectra of the cupric complexes formed with ligands **L1** (A) and **L3** (B) and of the mercuric complex formed with **L2** (C). Solvent: CH_3CN/CH_3OH (1/1 v/v); positive mode. (a) $[Cu^{2+}]_0$ or $[Hg^{2+}]_0 = [\mathbf{L}]_0 = 5 \times 10^{-5}$ M; $V_c = 150$ V. The ESI-MS spectra were limited to the areas of interest. No peaks were detected in the excluded m/z regions.
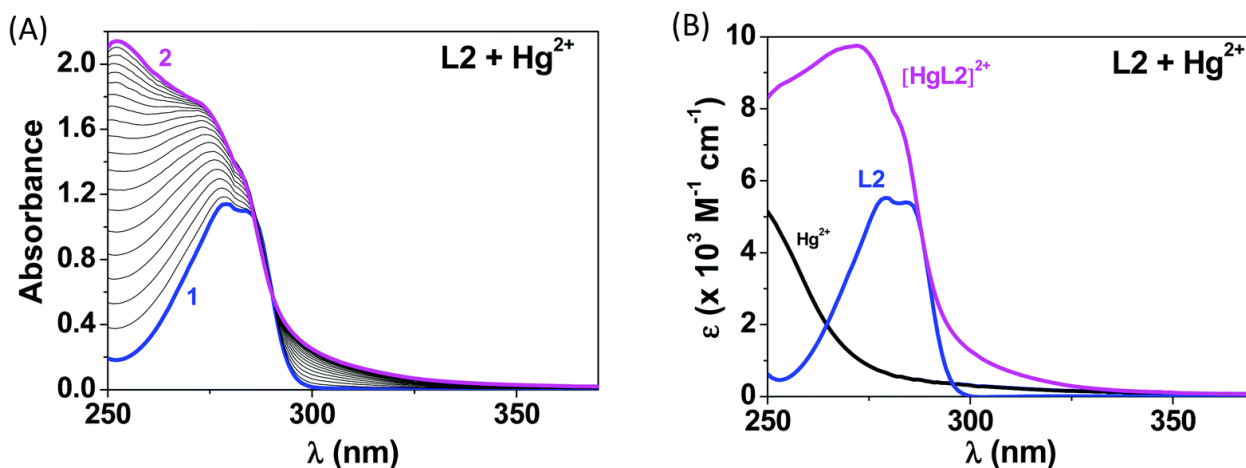
Fig. 5. (A) Absorption spectrophotometric titration of ligand **L2** by Hg^{2+} and (B) absorption electronic spectra of **L2**, Hg^{2+} and the metal complex $[HgL2]^{2+}$. Solvent: CH_3CN/CH_2Cl_2 (1/1 v/v); $I = 0.01$ M Et_4NNO_3; $T = 25.0(2)$ °C; $l = 1$ cm. $[L2]_0 = 10^{-4}$ M; (1) $[Hg^{2+}]_0/[L2]_0 = 0$; (2) $[Hg^{2+}]_0/[L2]_0 = 2$. The absorption spectra are not corrected for the dilution effects.
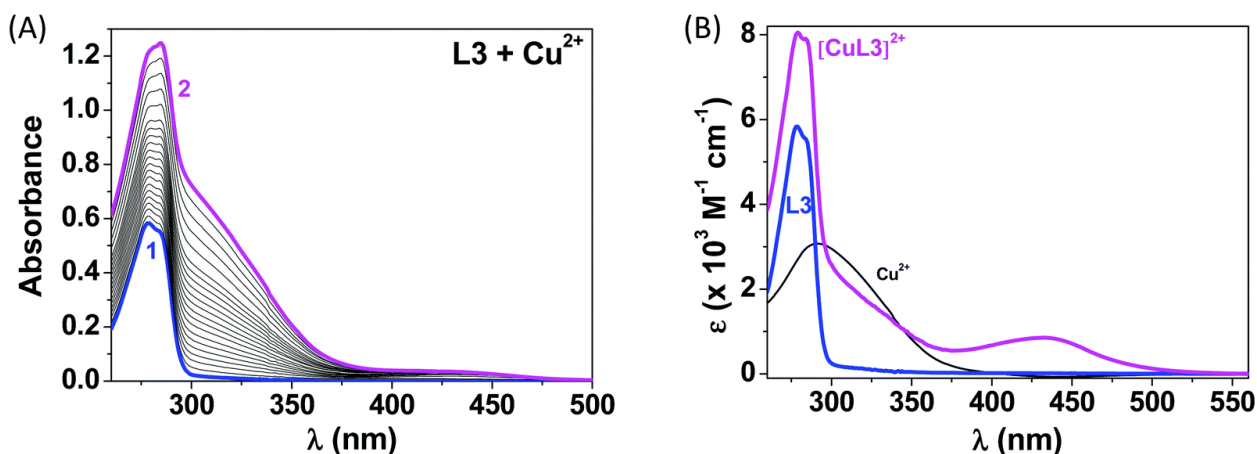
Fig. 6. (A) Absorption spectrophotometric titration of ligand **L3** by Cu^{2+} and (B) absorption electronic spectra of **L3**, Cu^{2+} and the metal complex $[CuL3]^{2+}$. Solvent: CH_3CN/CH_2Cl_2 (1/1 v/v); $I = 0.01$ M, Et_4NNO_3; $T = 25.0(2)$ °C; $l = 1$ cm. $[L3]_0 = 10^{-4}$ M; (1) $[Cu^{2+}]_0/[L3]_0 = 0$; (2) $[Cu^{2+}]_0/[L2]_0 = 2.5$. The absorption spectra are not corrected for the dilution effects.

Whatever the ligand considered, the formation of the Hg^{2+} monochelates are always characterised by the appearance of a broad and intense absorption band in the UV region ($\lambda_{max} < 260$ nm, Fig. 5) that is attributed to a S → Hg^{2+} charge transfer process (LMCT), which confirms the strong involvement of the sulphur atom to the Hg^{2+} binding. On the other hand, the absorption titration of **L1–L3** with $Cu(NO_3)_2$ evidenced the formation of additional absorptions in the UV (intense $(\sigma)S \rightarrow Cu^{2+}$ CT at ~330–340 nm) and visible regions (weak $(\pi)S$-to-Cu^{2+} CT at ~430 nm, Fig. 6).[26] The complexation titrations of Cd^{2+} were characterized solely by weak variations of the $\pi \rightarrow \pi^*$ transitions centred on the calix[4]arene unit. Irrespective of the ligand used, no significant variation was observed with Zn^{2+}. The statistical analysis[27–29] of the spectrophotometric data allowed us to clearly characterise and quantify the formation of monometallic monochelates (Table 3) and to calculate their corresponding electronic spectra (Fig. 5B and 6B, see also Fig. S3–S22, ESI,† for the other systems). The main absorption spectrophotometric characteristics for all the systems considered in this work are provided in Table 4.

Table 3. Logarithmic values of the stability constants (log $K_{[ML]}^{2+}$) of the monometallic (M = Hg^{2+}, Cu^{2+}, Cd^{2+} and Zn^{2+}) complexes formed with ligands **L1**, **L2** and **L3**[c]

Equilibrium	log $K_{[ML]}^{2+}$ (±3σ)		
	L1	**L2**	**L3**
$\mathbf{L} + Hg^{2+} \xrightleftharpoons{K_{[HgL]^{2+}}} [HgL]^{2+}$	3.6(2)[a]	5.4(3)[a]	5.5(4)[a]
	3.34(3)[b]	5.4(3)[b]	6.1(5)[b]
$\mathbf{L} + Cd^{2+} \xrightleftharpoons{K_{[CdL]^{2+}}} [CdL]^{2+}$	2.8(5)[a]	3.6(6)[a]	3.5(6)[a]
	3.0(5)[b]	4.1(6)[b]	3.3(2)[b]
$\mathbf{L} + Cu^{2+} \xrightleftharpoons{K_{[CuL]^{2+}}} [CuL]^{2+}$	4.3(3)[a]	≤1.6[a]	4.7(5)[a]
	4.3(3)[b]	nd[b]	4.62(5)[b]
$\mathbf{L} + Zn^{2+} \xrightleftharpoons{K_{[ZnL]^{2+}}} [ZnL]^{2+}$	nd[b]	~0.7[b]	3.2(2)[b]

[a] From UV-Vis absorption spectrophotometry. [b] From spectrofluorimetry. [c] Solvent: CH$_3$CN/CH$_2$Cl$_2$ (1/1 v/v); I = 0.01 M (Et$_4$NNO$_3$); T = 25.0(2) °C. The errors are estimated to be ±3σ with σ = standard deviation. nd = not determined under our experimental conditions.

Inspection of Table 4 allowed drawing other valuable information with respect to the mode of divalent metal binding with **L1–L3**. Metal complexation of the divalent heavy metals Hg^{2+}, Cu^{2+} and Cd^{2+} by **L1–L3** usually leads to hyperchromic shifts of the $\pi \to \pi^*$ transitions centred on the calix[4]arene unit with no bathochromic or hypsochromic variation. Moreover, the Hg^{2+} or Cu^{2+}binding is accompanied by the formation of absorption bands that can be attributed to ligand $\to$ metal charge transfer transitions. These LMCT bands are enlightening spectroscopic reporters for the characterization and the quantification of the Hg^{2+} and Cu^{2+} metal complexes with **L1–L3**. In the case of the Hg^{2+} cation,[30,31] large and intense S $\to$ Hg^{2+} CT absorption bands in the middle UV region (251 nm and a shoulder at ~291 nm for [HgL1]$^{2+}$; ~265 nm and shoulders at ~295 nm for [HgL2]$^{2+}$ and [HgL3]$^{2+}$) clearly reflect the involvement of the thiophosphates (**L1**) or the thiocrown ethers (**L2** and **L3**) in the Hg^{2+} recognition process. Our spectrophotometric data are also in agreement with the S(thiolate) $\to$ Hg^{2+} CT of metalloproteins or model complexes that typically range from 230 nm to 300 nm.[32–34] The strong and comparable absorptivities of the S $\to$ Hg^{2+} CT for the mercuric complexes with **L2** and **L3** strongly suggest the participation of 3 thioether units (*i.e.* tricoordinated mercuric species). Dicoordinated thiolate Hg^{2+} species are usually characterized by the presence of LMCT transitions at higher energies (Hg(SEt)$_2$: λ_{max} = 228 nm, ε^{228} = 4800 M^{-1} cm^{-1} and λ_{max} = 282 nm, ε^{282} = 740 M^{-1} cm^{-1}; Hg(S^{i}Pr)$_2$: λ_{max} = 228 nm, ε^{228} = 3400 M^{-1}cm^{-1} and λ_{max} = 262 nm, ε^{262} = 650 M^{-1} cm^{-1}).[34] The unambiguous participation of only two thiophosphate units is in agreement with the blue shift ($\Delta\lambda$ = 12–14 nm, Table 4) of the S $\to$ Hg^{2+} CT absorptions with respect to the mercuric complexes with **L2** and **L3**. Furthermore, [HgL1]$^{2+}$ was found to be the less stable mercuric complex (log $K_{[HgL1]}^{2+}$ = 3.6(2)) within the ligand series examined in this work. The comparable CT spectral characteristics (Table 4) and stabilities measured for [HgL2]$^{2+}$ and [HgL3]$^{2+}$(log $K_{[HgL2]}^{2+}$ = 5.4(3) *versus* log $K_{[HgL3]}^{2+}$ = 5.5(4)) suggest a similar coordination environment. With respect to the HSAB classification,[35] the Hg^{2+} cation (soft metal cation with an ionic radius of 1.10 Å for CN 4 and 1.16 Å for CN 6) usually accommodates well with soft sulphur-containing ligands. Therefore, we assume the absence of interactions with the phenolic groups borne by the calix[4]arene platform.

Fig. 7 depicts the TPSSh/TZVP optimized geometries of the mercuric complexes with **L1–L3**. The [HgL1]$^{2+}$ complex is predicted to present an almost linear coordination around the metal ion (CN 2), with a S1–Hg1–S2 angle of 179.2° and Hg–S distances of 2.43 Å (Table S1, ESI†). Conversely, the

[Hg**L2**]$^{2+}$ complex displays a three-coordinate Hg^{2+} ion with a T-shape coordination environment (S1–Hg1–S2, 161.5°; S1–Hg1–S3, 84.3°; S2–Hg1–S3, 84.3°) and Hg–S distances in the range of 2.59–2.81°. Finally, the [Hg**L3**]$^{2+}$ complex is four-coordinated, with two bond distances (Hg1–S1, 2.59; Hg1–S2, 2.61 Å) being clearly shorter than the remaining two (Hg1–S3, 2.73; Hg1–S4, 2.79 Å). The S–Hg1–S angles fall within the range of 81.8–148.9°, with the largest angle corresponding to S1–Hg1–S2. Thus, the structures calculated for the three complexes highlight the trend of Hg^{2+} to favour linear coordination.

Table 4. Spectrophotometric characteristics (UV-Vis absorption) of L1–L3 and their corresponding metal complexes with Hg^{2+}, Cu^{2+} and Cd^{2+a}

| Cation | Species | λ^{abs}_{max} (ε) [nm (M^{-1} cm^{-1})] | | |
		Transitions π–π* and n–π*	LMCT S → Hg^{2+}	LMCT S → Cu^{2+}
—	**L1**	275 (8010)		
		282 (7550)		
—	**L2**	279 (5530)		
		284 (5400)		
—	**L3**	279 (5500)		
		284 (5280)		
Hg^{2+}	[Hg**L1**]$^{2+}$	273 (13 390) sh	250 (39 260)	
		282 (8370)	251 (32 750)^b	
			291 (950) sh ^{b}	
	[Hg**L2**]$^{2+}$	272 (9750)	265 (5480)^b	
		283 (7490)	296 (1100) sh ^{b}	
	[Hg**L3**]$^{2+}$	275 (8370)	263 (6650)^b	
		284 (9000)	295 (2340) sh ^{b}	
Cu^{2+}	[Cu**L1**]$^{2+}$	276 (10 070)		317 (1890) sh 432 (487)
		282 (9960)		
	[Cu**L2**]$^{2+}$	^{c}	^{c}	^{c} ^{c}
	[Cu**L3**]$^{2+}$	279 (8050)		329 (1270) sh 432 (856)
		284 (7900)		
Cd^{2+}	[Cd**L1**]$^{2+}$	276 (9330)		
		284 (8980)		
	[Cd**L2**]$^{2+}$	278 (5960)		
		285 (5580)		
	[Cd**L3**]$^{2+}$	279 (6700)		
		284 (6330)		

^{a} Solvent: CH$_3$CN/CH$_2$Cl$_2$ (1/1 v/v); $T = 25.0(2)$ °C. The errors on λ and ε are estimated to be ±1 nm and ±5%, respectively. ^{b} Estimated values from the differential electronic spectra. ^{c} The [Cu**L2**]$^{2+}$ complex is characterized by a d–d absorption band (Cu^{2+}) at 667 nm ($\varepsilon^{667} = 218$ M^{-1}cm^{-1}). The Zn^{2+} complexes were not characterized by UV-Vis absorption spectrophotometry.

The 30 lowest excited states of [Hg**L2**]$^{2+}$ were calculated using TDDFT at the TPSSh/TZVP level to rationalise the spectral changes observed in the absorption spectra upon metal ion complexation (see computational details below). The energy of the lowest excited state was calculated to be 509 nm (oscillator strength $f = 0.008$), while the 30th excited state was calculated to be 245.7 nm. Within this spectral range, the absorption spectrum is predicted to be dominated by the excitation to excited state 19, which is calculated to be at 268.1 nm ($f = 0.30$). The energy of this excited state is in excellent agreement with the maximum of the absorption spectrum observed at 265 nm (Table 4). The oscillator strengths calculated for the remaining excited states were considerably lower (<0.05). The excited state giving rise to the absorption at 268.1 nm is

dominated by electron excitations from MOs 165, 166 and 167 to the LUMO (MO 177). Inspection of these MOs reveals that the composition of the LUMO is dominated by the Hg 6s orbital with some additional contribution from the S lone pairs (Fig. S35, ESI†). On the other hand, MOs 165, 166 and 167 possess very important contributions of the S lone pairs. Thus, our TDDFT calculations confirm the LMCT origin of the absorption bands that dominate the absorption spectra of the Hg^{2+} complexes in the region of 250–300 nm.
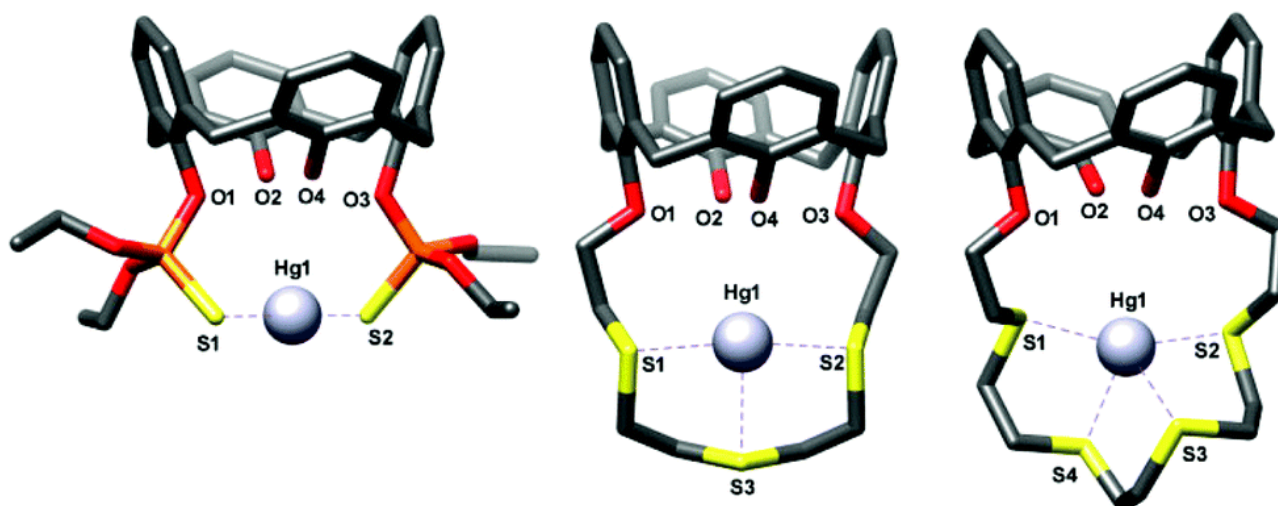
Fig. 7. Optimized (TPSSh/TZVP) geometries for the mercuric complexes with ligands **L1**, **L2** and **L3**. Hydrogens have been omitted for the sake of clarity.

The cupric complexes with **L1** and **L3** are clearly characterized by CT absorption bands in the UV ((σ)S $\rightarrow$ d(Cu^{2+})) domain, while the weaker absorption seen for $[CuL1]^{2+}$ and $[CuL3]^{2+}$ in the visible region can be likely related to ((π)S $\rightarrow$ d(Cu^{2+})) CT (*i.e.* DFT calculations suggest the non-participation of the phenol groups in $[CuL3]^{2+}$, Fig. 12). Intense absorption shoulders at 317 nm ($[CuL1]^{2+}$, Fig. S12, ESI†) and 329 nm ($[CuL3]^{2+}$, Fig. 6) are in agreement with the related spectral data reported for symmetrical pentadentate thioaza[36] or unsymmetrical NSN[37] systems.[26] In contrast with Hg^{2+}, which preferentially binds to soft sulphur-based ligands, Cu^{2+} is characterized by a smaller ionic radius (0.71 Å for CN 4 and 0.87 Å for CN 6; borderline HSAB character) and might not be stabilized by only thioether or thiophosphate coordination units. It is then expected that the phenol units of the calixarene scaffold could participate in the Cu^{2+} binding.[38–41] $[CuL1]^{2+}$ (log $K_{[CuL1]}^{2+}$ ~ 4.3(3)) and $[CuL3]^{2+}$ (log $K_{[CuL3]}^{2+}$ ~ 4.7(5)) display comparable complexation constants, while a low stability is measured for $[CuL2]^{2+}$ (log $K_{[CuL2]}^{2+}$ ~ 1.6) which prevents accurate assessment of its corresponding absorption properties. The absorption titrations of the concentrated solutions of **L2** by Cu^{2+} allowed monitoring the spectral alterations of the Cu^{2+} d–d transitions. The $[CuL2]^{2+}$ species is characterized by d–d transitions centred at ∼670 nm.

We next took advantage of the fluorescence emission properties of **L1–L3** to investigate their interactions with the heavy metal ion series. Scarce examples of calix[4]arene derivatives being intrinsically fluorescent as seen for **L1–L3** have been reported in the literature. In contrast, many fluorescent sensors have been engineered by introducing conventional organic fluorophores (9-cyanoanthracene, dioxycoumarin, dansyl, anthrylmethyl, bipyridines, *etc.*) to calix[*n*]arene scaffolds.[14a,42,43] These fluoro-ionophores, designed to track metallic cations of relevance for environmental or health issues (Cs^+, Hg^{2+}, Pb^{2+}, Cd^{2+}, Cu^{2+}, Zn^{2+}, *etc.*), take advantage of the metal chelation properties of the calixarene moiety (providing the fact that the calixarene unit has been judiciously modified) and the reporting properties of the coordination process by the fluorescent moieties. Alternatively, calix[4]arene conjugates[44] bearing salicyl-imino binding sites were found

to become fluorescent (OFF–ON systems) upon Cd^{2+} (ref. 45) or Zn^{2+} (ref. 46) complexation. These metal complexes have been advantageously used in a broad range of biological applications[47] such as selective recognition of amino acids[45,48] or chemo-sensing of (pyro)phosphates.[46b] In particular, the Zn^{2+} and Cd^{2+} complexes displayed interesting fluorescence emission owing to the preclusion of photoinduced electron transfer (PET) processes upon implication of the lone pair of imine electrons for metal complexation.[14c,49] Alternatively, complexation of redox active metal ions such as Cu^{2+} or Hg^{2+} led to fluorescence quenching.[50] The **L1–L3** ligands were demonstrated to display both fluorescence emission and heavy metal binding capacities. The complexation of the Hg^{2+} or Cu^{2+} electroactive metal ions (Fig. 8 and 9) led to drastic quenching of the ligand centred fluorescence emission, while the redox inert Cd^{2+} or Zn^{2+} weakly altered these emissions (Fig. 10). Altogether, these data suggest a photoinduced electron transfer (oxidative L → M electron transfer in the excited state) leading to a static inhibition process. This spectral feature stands in contrast with a 1,3-di-capped calix[4]arene conjugate of salicylidene that shows a selective and drastic fluorescence emission increase (OFF–ON Hg^{2+} chemosensor) in the presence of Hg^{2+} ions.[51] Hg^{2+} was found to be bound to four phenolic oxygens and one imine nitrogen resulting in a highly distorted square pyramidal geometry. The stability constants determined for **L1–L3** by fluorimetric titrations were found to be in good agreement with those determined by absorption spectrophotometry (Table 4). Ligands **L1–L3**, therefore, play the role of selective ON–OFF fluorescent chemosensors with respect to Hg^{2+} and Cu^{2+}. This stands in contrast to fluoroionophores[16,17] based on the azathiocrown ether for which Hg^{2+} binding affects the intramolecular charge transfer (ICT) and consequently induces spectral shifts.

Heavy metals binding properties

Hg^{2+} ($5d^{10}$) and Cd^{2+} ($4d^{10}$) cations formed the more stable complexes upon binding with the sulphur-rich thiocrown ethers **L2**(3S) and **L3** (4S) as a consequence of their large coordination cavity (Fig. 11). In contrast, the corresponding species with the thiophosphate-based ligand **L1** are one to two orders of magnitude less stable due to the presence of only two P=S coordination units (dicoordinated mercuric species, Table 3). Further evidence was provided by the ^1H NMR titration of **L1** by Hg^{2+} (Fig. S36, ESI†) which shows that: (i) the chemical shifts of protons borne by the calix[4]arene are not affected upon metal ion addition (*i.e.* the cone conformation is preserved); (ii) an upfield shift is observed for the OH groups; and (iii) a downfield shift occurs for the methylenic protons of the ethoxy substituents. These NMR data confirmed the absence of Hg^{2+} complexation by the phenolic groups and the retention of the cone conformation of the calix[4]arene (Fig. 7). These data are in agreement with a previous NMR study on **L1′** (**L1** analogue displaying *p-tert*-butyl substituents on the lower rim)[10] and its Ag^+ complexes, which demonstrated that the cone conformation was maintained during the complexation and that the Ag^+ cation was only bound by the sulphur atoms of the thiophosphate units.

Surprisingly, the binding constants of **L1′** with divalent metal ions were found to be higher in pure CH_3CN (Hg^{2+}: $\log K_{[HgL1']}^{2+} = 7.4(5)$; Zn^{2+}: $\log K_{[ZnL1']}^{2+} = 3.6(2)$; Cd^{2+}: $\log K_{[CdL1']}^{2+} = 3.7(1)$) with respect to our data (Table 3). In addition to the presence of *tert*-butyl substituents (on the lower rim), which can markedly alter the upper binding site, these data also suggest the role of the solvation of the free metal ions or corresponding complexes, as such complexes could display dual inorganic–organic complexation behaviours.[22b] For instance, the stability of the metal–thioether complexes (di-*n*-alkylsulfide or macrocyclic ligands such as [9]aneS3, [12]aneS4 or [14]aneS4) were found to be much lower in DMSO with respect to acetonitrile mostly because of the much stronger solvation of metals in DMSO.[52] No significant difference could be observed between **L2** and **L3** in terms of the stability of the Hg^{2+} complexes. Our DFT calculations indeed indicate that two of the sulphur atoms of the ligand (S1 and S2) provide the strongest interaction with Hg^{2+}, while the remaining one (**L2**) or two (**L3**) sulphur donor atoms provide a rather weak coordination (Fig. 7). The participation of the phenolic units in the complexation of Hg^{2+} and Cd^{2+} was excluded due to their particular electronic properties (*i.e.* borderline hardness/softness character) and the absence of specific spectroscopic signatures.
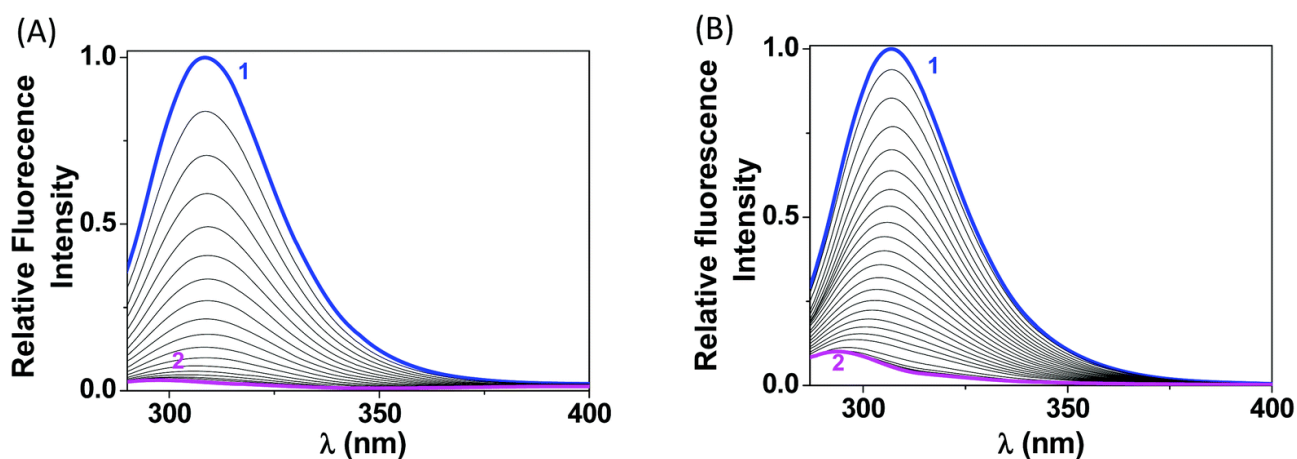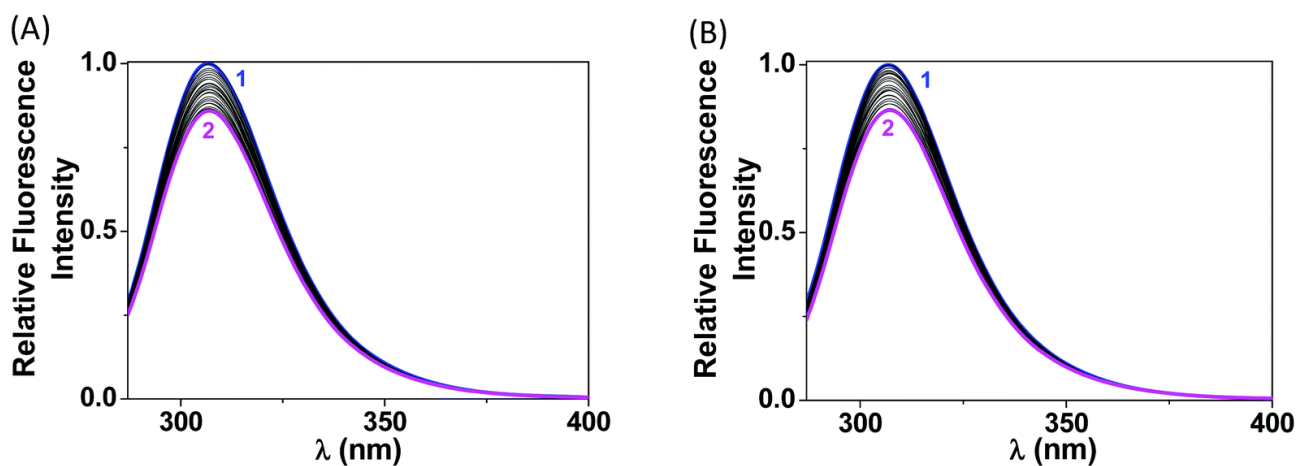
Fig. 8. Fluorescence emission titration of (A) **L2** (λ_{exc} = 287 nm) and (B) **L3** (λ_{exc} = 289 nm) by Hg^{2+}. Solvent: CH_3CN/CH_2Cl_2 (1/1 v/v); I = 0.01 M Et_4NNO_3; T = 25.0(2) °C; ℓ = 1 cm. (A) $[\text{L2}]_0 = 10^{-4}$ M; (1) $[Hg^{2+}]_0/[\text{L2}]_0 = 0$; (2) $[Hg^{2+}]_0/[\text{L2}]_0 = 2$. (B) $[\text{L3}]_0 = 10^{-4}$ M; (1) $[Hg^{2+}]_0/[\text{L3}]_0 = 0$; (2) $[Hg^{2+}]_0/[\text{L3}]_0 = 3$. The emission spectra are not corrected from the dilution effects.
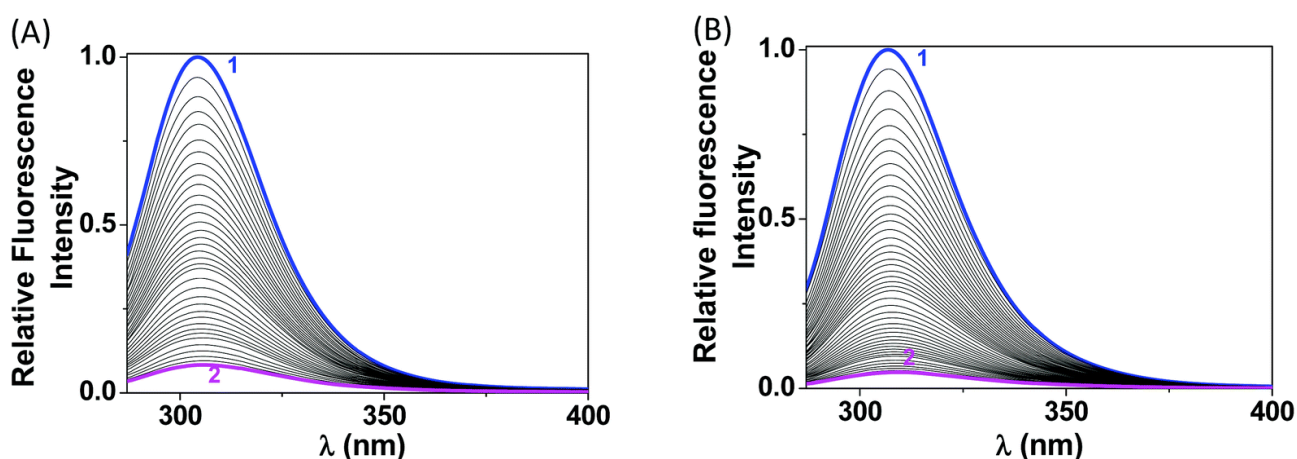
Fig. 9. Fluorescence emission titration of (A) **L1** (λ_{exc} = 287 nm) and (B) **L3** (λ_{exc} = 287 nm) by Cu^{2+}. Solvent: CH_3CN/CH_2Cl_2 (1/1 v/v); I = 0.01 M Et_4NNO_3; T = 25.0(2) °C; ℓ = 1 cm. (A) $[\text{L1}]_0 = 10^{-4}$ M; (1) $[Cu^{2+}]_0/[\text{L1}]_0 = 0$; (2) $[Cu^{2+}]_0/[\text{L1}]_0 = 2.5$. (B) $[\text{L3}]_0 = 10^{-4}$ M; (1) $[Cu^{2+}]_0/[\text{L3}]_0 = 0$; (2) $[Cu^{2+}]_0/[\text{L3}]_0 = 3.7$. The emission spectra are not corrected for the dilution effects.

In acetonitrile, the tridentate [9]aneS3 ligand was found to be able to form complexes with all the target cations (Zn^{2+}, Cd^{2+} or Hg^{2+}), while the monodentate Et_2S only reacted with Hg^{2+}. [9]AneS3 forms complexes with Hg^{2+} of much higher stability than the other target cations (*i.e.* Cd^{2+} and Zn^{2+}) in agreement with the data obtained for **L2** and **L3**. Monometallic ML_i (i = 1, 2) complexes are formed with all the metal ions investigated, where the affinity order is $Hg^{2+} > Ag^+ > Cd^{2+} \approx Zn^{2+}$ with L = [9]aneS3 and $Hg^{2+} > Ag^+$ when L = Et_2S.[53] In solution or in the solid state,[54] all the three sulphur atoms of the [9]aneS3 macrocycle bind the metal ion in the $[Hg([9]aneS3)]^{2+}$ or $[Hg([9]aneS3)_2]^{2+}$ species, which maintains a distorted octahedral geometry around the metal ion. This is the consequence of polythioether macrocycles that have the ability to force different coordination modes on the Hg^{2+} centre (hexa-coordination), in contrast to the tetrahedral and linear geometries that are usually observed in the coordination chemistry of this ion.[25,54] **L2** and **L3** stand in an interesting contrast since the calix[4]arene scaffold precludes the formation of such species and only monometallic monochelate species are observed (Table 3).

Fig. 10. Fluorescence emission titration of **L3** by (A) Cd^{2+} (λ_{exc} = 287 nm) and (B) Zn^{2+} (λ_{exc} = 287 nm). Solvent: CH_3CN/CH_2Cl_2(1/1 v/v); I = 0.01 M Et_4NNO_3; T = 25.0(2) °C; ℓ = 1 cm. (A) [**L3**]$_0$ = 10^{-4} M; (1) [Cd^{2+}]$_0$/[**L3**]$_0$ = 0; (2) [Cd^{2+}]$_0$/[**L3**]$_0$ = 7.0. (B) [**L3**]$_0$ = 10^{-4} M; (1) [Zn^{2+}]$_0$/[**L3**]$_0$ = 0; (2) [Zn^{2+}]$_0$/[**L3**]$_0$ = 9.4. The emission spectra are not corrected for the dilution effects.
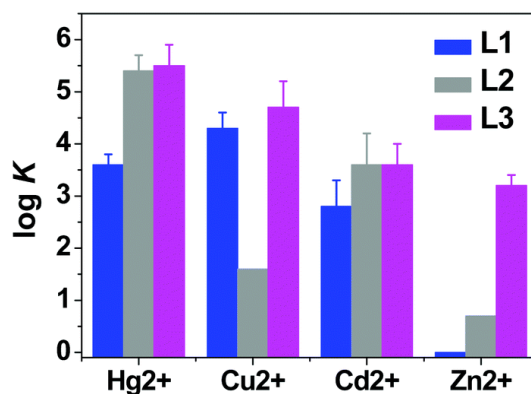

Fig. 11. Schematic representation of the stability constants of the metal complexes with ligands **L1–L3**.

Cu^{2+} ($3d^9$) and Zn^{2+} ($3d^{10}$) display larger charge densities, which confer them different coordination properties. They possess a good affinity for nitrogen-based (or oxygen-) ligands and consequently afford less stable metal complexes with the sulphur-rich ligands **L1–L3** when compared to the Hg^{2+} complexes. On the other hand, Cu^{2+} and Zn^{2+} usually lead to complexes that involve coordination numbers ranging between 4 and 6. The $3d^9$ configuration of Cu^{2+} experiences Jahn–Teller distortions[55,56] in a cubic symmetry environment (octahedral and tetrahedral). This often leads to a geometric distortion[57] with an elongation or shortening of the metal–ligand distances along the z-axis.[58] In contrast, the $3d^{10}$ electronic configuration of Zn^{2+} does not involve any stabilization by the ligand field. Its stereochemistry is therefore only determined by the size effects, electrostatic interactions and covalent bonding forces.[25] As a consequence, only **L3** (4S thiocrown ether) is able to lead to stable Zn^{2+}complexes. Our physico-chemical data further show that **L1** (two thiophosphates) and **L3** (4S thiocrown ether) lead to rather stable Cu^{2+} complexes when compared to the corresponding Hg^{2+} ones.

DFT calculations (Fig. 12, see also Table S2, ESI†) further suggest that the binding of **L1** to the Cu^{2+} ion occurs through three oxygen atoms of the calixarene unit (O1, O2 and O4) and the two sulphur atoms (S1 and S2). The fourth oxygen atom of the calixarene unit provides a weak coordination to the metal ion (Cu1–

O3 = 2.62 Å). In the case of [Cu**L2**]$^{2+}$ only one oxygen atom of the ligand is involved in metal ion coordination according to the DFT results (Cu–O1 = 2.134 Å), the metal coordination environment being fulfilled by the three sulphur atoms of the ligand that provide Cu–S distances in the range of 2.39–2.43 Å. The metal coordination environment is predicted to be distorted square planar, with *cis* angles in the range of ~83–106°. In contrast, the calculated structure of [Cu**L3**]$^{2+}$ displays a S4 coordination in which the oxygen atoms of the ligand are not involved in metal ion coordination. All complexes retain the cone conformation and present similar coordination environments.
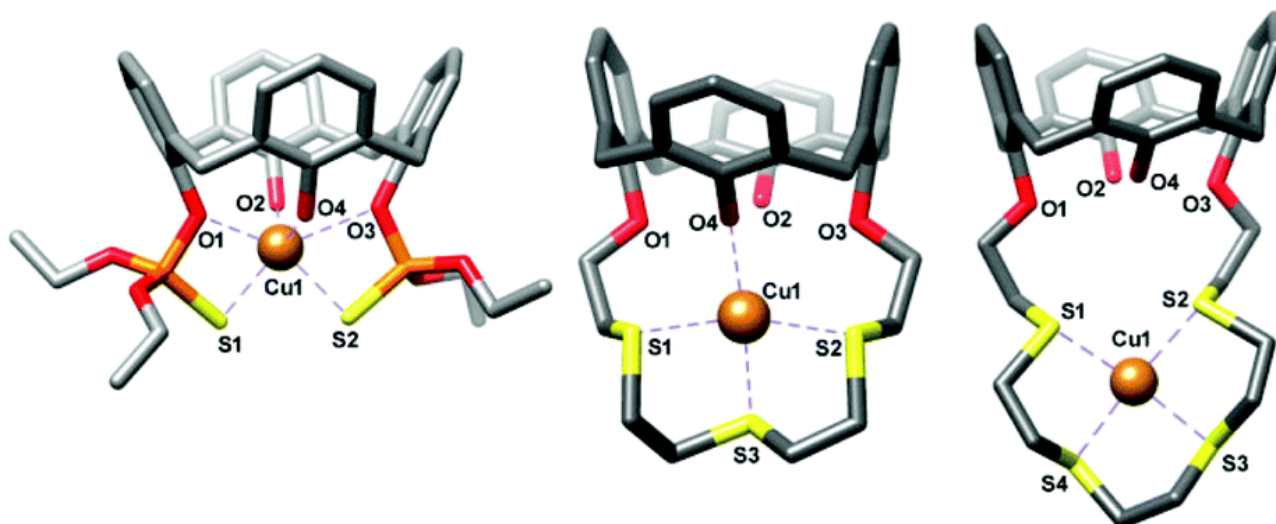
Fig. 12. Optimized (TPSSh/SVP) geometries of the cupric complexes with **L1** (S$_2$O$_2$), **L2** (S$_3$O) and **L3** (S$_4$).

Ligand **L2** (S$_3$O coordination according to DFT) afforded the less stable cupric complex (destabilization of more than 3 orders of magnitude when compared to **L3**), which may reflect strong structural and steric constraints when the size of the thiocrown ether is reduced. The strain energy of the ligands in the metal complexes, estimated as the energy difference between the minimum energy conformation of the ligand and that of the ligand found in the complex, amounts to 50.7 and 49.0 kJ mol^{-1} for **L2** and **L3**, respectively. Being small, these values suggest that the higher strain energy of the ligand might be responsible, at least in part, for the lower stability of the cupric complex with **L2**. However, the electrostatic factors likely play a major role, as the coordination of the Cu^{2+} ion by **L2** brings the metal ion relatively close to the –OH group of a phenol unit. The same effect was also observed for the Zn^{2+} complexes with **L2**–**L3** with a destabilization of ~2.5 orders of magnitude upon shortening of the thiocrown ether chain length (Table 3). The larger size of the thiocrown ether unit likely facilitates the S4 coordination in [Cu**L3**]$^{2+}$, resulting in the increased stability of the complex in comparison with [Cu**L2**]$^{2+}$. Interestingly, only **L3** satisfactorily follows the Irving–Williams series[59] which predicts the relative affinity of metallic cations for an organic ligand as follows: Hg^{2+} ≫ Cu^{2+} ≫ Cd^{2+} > Zn^{2+}.

Conclusions

This physico-chemical and spectroscopic investigation allowed evaluation of the heavy metal (Hg^{2+}, Cd^{2+}, Cu^{2+} and Zn^{2+}) complexation properties of three sulphur-rich calix[4]arene receptors (**L1**–**L3**). These chelators containing thiocrown ethers or thiophosphate fragments are characterized by UV electronic transitions (π–π* and n–π*) as well as ligand-to-metal CT transitions that emerged upon binding of redox

active metal ions such as Hg^{2+} and Cu^{2+} and provided valuable information on the stoichiometry and nature of the metal complexes. The presence of CT absorptions $S \rightarrow Hg^{2+}/S \rightarrow Cu^{2+}$ also allowed us to easily track the formation of the corresponding complexes and to point out the implicated coordination sites. Besides, these calix[4]arene receptors displayed fluorescence emission properties that were beneficially used to characterize and quantify the targeted metal complexes. In particular, the electroactive metals Hg^{2+} and Cu^{2+} were able to effectively quench the fluorescence of the binders likely by a PET mechanism that involves an electron transfer from the chromophore to the metal in the excited states. Regardless of the nature of the ligand, monometallic monochelates were only observed as assessed by the ESI-MS approach and in excellent agreement with the spectrophotometric data. **L2** and **L3** receptors, displaying soft thiocrown ether moieties, led to stable mercuric complexes with respect to the other investigated metals ions. The tetradentate ligand **L1**, however, forms more stable cupric complexes than with Hg^{2+} ions. The denticity of the ligand has a strong impact on the thermodynamic stability of the corresponding complexes with Cu^{2+} and Zn^{2+}, while the number of sulphur atoms of the thiocrown ether unit strongly affects the stability of the mercuric complex. This study allowed us to suggest the exclusive involvement of the thiolates or thiophosphate units in the complexation and stabilization of Hg^{2+} and Cd^{2+} complexes, while the phenol units of the calix[4]arene base are proposed to be weakly involved, in combination with the sulphur-containing units, in the recognition process of the hard cations such as Cu^{2+} and Zn^{2+} by **L1** and **L2**. In the case of **L3** DFT calculations suggest however a S4 coordination of Cu^{2+} that could explain the higher stability of the $[CuL3]^{2+}$ complex in comparison to the analogue with **L2**. Ligand **L1**–**L3** receptors thus constitute interesting chelating scaffolds for further development of efficient systems for chelation and extraction of trace elements such as the toxic Hg^{2+} ion. Besides, their intrinsic photophysical properties might be advantageously used to track and quantify these processes.

Experimental section

<u>Materials and methods</u>

All reagents and solvents were commercial grade and used without further purification. Column chromatographic purifications were performed on silica (60–200 μm, Merck). K_2CO_3 was flash dried under vacuum prior to use. Calix[4]arene,[60] compounds **1**(1,3-di(chloroethoxy)-calix[4]arene)[18] and **L3**[18] were prepared according to the literature procedures. ^{1}H- and ^{13}C-NMR experiments were performed on Bruker AC 200 and Avance 300 spectrometers working at 200 and 300 MHz respectively for [1]H. Chemical shifts are given in part per million relative to residual protonated solvents.[6] ^{31}P-NMR spectra (161.9 MHz) were recorded on an Avance 400 Bruker spectrometer. Elemental analysis and mass spectrometry analysis were performed at the Service central d'analyses of the University of Strasbourg and the X-ray crystal structures were determined at the service de cristallographie of the University of Strasbourg.

Synthesis of L1. In a 250 mL round flask, fitted with a condenser and under a N_2 atmosphere, calix[4]arene (1.70 g, 4.0 mmol) was slowly dissolved in 120 mL of acetone. K_2CO_3 (0.66 g, 4.8 mmol) was added. After 30 min diethylchlorothiophosphate (1.56 g, 8.0 mmol) was added and the mixture was refluxed for 3 days. Acetone was removed under reduced pressure and the residue was partitioned between water and CH_2Cl_2. The pH of the aqueous phase was adjusted to *ca.* 7.0 by addition of diluted HCl and the organic phase was recovered, dried over Na_2SO_4, filtered and concentrated until a viscous residue was obtained. Upon addition of MeOH, a white solid precipitated, which was filtered and dried under reduced pressure to give **L1** (2.42 g, 3.32 mmol) in 83% yield. ^{1}H-NMR (CDCl$_3$, 300 MHz): δ 7.10 (d, 4H, J = 7.5 Hz), 6.76 (d, 4H, J = 7.5 Hz), 6.69–6.73 (m, 4H), 5.57 (s, 2H), 4.48 (d, 4H, J = 13.0 Hz), 4.33 (m, 8H), 3.45 (d, 4H, J = 13 Hz), 1.39 (t, 12H, J = 7.0 Hz). ^{13}C-NMR (CDCl$_3$, 100 MHz): δ 152.8, 145.1 (d, J^{P-C} = 8.0 Hz), 132.6 (d, J^{P-C} = 2.0 Hz), 129.2, 128.7 (d, J^{P-C} = 17.5 Hz), 125.9, 119.7, 65.5 (d, J^{P-C} = 6.2 Hz), 32.4, 16.1 (d, J^{P-C} = 7.6 Hz).^{31}P-NMR

(CDCl$_3$, 161.9 MHz): δ 64.06. ESI$^+$/MS (CH$_2$Cl$_2$): m/z 729.19 ([M + H]$^+$, 100%). Anal. calcd for C$_{36}$H$_{42}$O$_8$P$_2$S$_2$: C, 59.33; H, 5.81. Found: C, 59.52; 5.73%.

Synthesis of L2. In a 500 mL round bottom flask fitted with a condenser under a nitrogen atmosphere, thiodiethanethiol (412 mg, 2.67 mmol) and KOH (270 mg, 4.80 mmol) were refluxed for 10 min. in a mixture of benzene (200 mL) and DMF (100 mL). Compound **1** (1.10 g, 2.0 mmol) was added and the reflux was prolonged for 4 h. The solvents were removed under reduced pressure and the residue was partitioned between CH$_2$Cl$_2$ and water. The pH of the aqueous layer was decreased to 7 with 1 M aqueous HCl, the organic phase was decanted, dried over Na$_2$SO$_4$, filtered and evaporated to dryness. Ligand **L2** was purified by column chromatography over SiO$_2$ using cyclohexane/CH$_2$Cl$_2$ (4/6) and was obtained as a white solid (920 mg, 73%). ^{1}H-NMR (CDCl$_3$, 300 MHz): δ 7.31 (s, 2H), 7.07 (d, 4H, J = 7.5 Hz), 6.82 (d, 4H, J = 7.5 Hz), 6.73–6.67 (m, 4H), 4.36 (d, 4H, J = 13 Hz), 4.17 (t, 4H, J = 6.5 Hz), 3.42 (d, 4H, J = 13 Hz), 3.25 (t, 4H, J = 6.5 Hz), 3.01–3.10 (m, 8H). ^{13}C-NMR (CDCl$_3$, 75 MHz): δ 153.0, 151.9, 133.1, 129.0, 128.6, 128.4, 125.4, 119.3, 76.2, 34.0, 32.9, 32.4, 31.3. ESI$^+$/MS (CH$_2$Cl$_2$): m/z 631.15 ([M + H]$^+$, 100%). Anal. calcd for C$_{36}$H$_{38}$O$_4$S$_3$: C, 68.54; H, 6.07. Found: C, 68.16; 6.18%.

Physico-chemical measurements

Solvents and materials. For the sake of solubility of the metallic salts (Hg^{2+}, Pb^{2+}, Cu^{2+} and Zn^{2+} as nitrate salts) and ligands (**L1–L3**), a mixed solvent made of CH$_2$Cl$_2$ and CH$_3$CN (50/50 v/v) was used. All the physico-chemical analyses were carried out with spectroscopic grade 1,2-dichloromethane and acetonitrile (Merck, 99.9%). All stock solutions (ligands and metals) were prepared by weighing the solid products using a AG 245 Mettler Toledo analytical balance (precision 0.01 mg) and the complete dissolution in the mixed solvent was achieved using an ultrasonic bath (Bandelin Sonorex RK102). The stock solutions of the divalent metal ions (Hg^{2+}, Cu^{2+}, Cd^{2+} and Zn^{2+}) were daily and freshly prepared from their corresponding nitrate salts (Hg(NO$_3$)$_2$·H$_2$O, Merck; Cu(NO$_3$)$_2$·3H$_2$O Fluka, >99%; Cd(NO$_3$)$_2$, Toulabo; Zn(NO$_3$)$_2$·4H$_2$O, Merck, >99%). All the solutions were protected from daylight to avoid any photochemical degradation. The ionic strength of the solutions used for the spectrophotometric (absorption and emission) titrations was adjusted to 0.01 M with tetraethylammonium nitrate (Et$_4$NNO$_3$, Merck, >99%). All the physico-chemical measurements were carried out at 25.0(2) °C.

UV-Vis absorption titrations. The absorption spectrophotometric titrations of the ligands **Li** (i = 1–3) were carried out in a Hellma quartz optical cell (1 cm or 0.2 cm). Microvolumes of concentrated metal (Hg^{2+}, Pb^{2+}, Cu^{2+} and Zn^{2+}) solutions (10^{-3} M for l = 1 cm and 2 × 10^{-2} M for l = 0.2 cm) were added to 2 mL (10^{-4} M for l = 1 cm) or 0.5 mL (10^{-3} M for l = 0.2 cm) of the ligand solutions with microliter Hamilton syringes (#710 and #750). Special care was taken to ensure that complete equilibration was attained. The corresponding UV-Vis spectra were recorded from 230 nm to 700 nm on a Kontron Uvikon 941 or Varian Cary 300 spectrophotometer maintained at 25.0(2) °C by the flow of a Haake NB 22 thermostat.

Luminescence titrations. The luminescence titrations of an aliquot of 2 mL of the ligands **Li** (i = 1–3; $\sim$10^{-3}–10^{-4} M) were carried out in a 1 cm Hellma quartz optical cell by addition of known microvolumes of the concentrated stock (10^{-3} M or 2 × 10^{-2} M) metal solutions (Hg^{2+}, Pb^{2+}, Cu^{2+} and Zn^{2+}) with microliter Hamilton syringes (#710 and #750). The excitation wavelength λ = 287–289 nm corresponds to an isosbestic point between the free ligands and the metal complexes or to the smallest absorbance amplitudes measured along the absorption spectrophotometric titrations. The luminescence spectra were recorded from 280 nm to 800 nm on a Perkin-Elmer LS-50B maintained at 25.0(2) °C by the flow of a Haake FJ thermostat. The light source was a pulsed xenon flash lamp with a pulse width at half peak height <10 μs and power equivalent to 20 kW. The slit width was set at 15 nm and 20 nm for the excitation and the emission, respectively.

Processing of the spectrophotometric data. The spectrophotometric data were processed with the Specfit programs, which adjust the stability constants and the corresponding extinction coefficients of the species

formed at equilibrium. Specfit[27–29] uses factor analysis to reduce the absorbance matrix and to extract the eigenvalues prior to the multiwavelength fit of the reduced data set according to the Marquardt algorithm.[62,63] The distribution curves of the various species were calculated using the Hyss program.[64]

Electrospray mass spectrometric measurements. The electrospray mass spectra of metal complexes with **L1–L3** were obtained with an Agilent Technologies 6120 quadrupole equipped with an electrospray (ESI) interface. Solutions ($[\textbf{L}]_0 = 5 \times 10^{-5}$M; $[\textbf{M}]_0/[\textbf{L}]_0 = 1–3$) of the metal complexes (Hg^{2+}, Cd^{2+}, Cu^{2+} and Zn^{2+}) with **L1–L3** have been prepared in a mixed solvent made of acetonitrile and methanol in the absence of any background salt. The sample solutions were continuously introduced into the spectrometer source with a syringe pump (Kd Scientific) with a flow rate of 300 μL h^{-1}. For electrospray ionization, the drying gas was heated at 250 °C and its flow was set at 6 L min^{-1}. The capillary exit voltage was fixed at 5 kV and the skimmer voltage was varied from 50 to 300 V in order to optimize the signal responses. Scanning was performed from $m/z = 100$ to 1500 and no significant fragmentation processes were observed under our experimental conditions.

Photophysical measurements. Fluorescence and excitation spectra were recorded in 1 cm^2 quartz Suprasil cells (Hellma) on a Horiba Jobin Yvon Fluorolog 3 spectrometer working with a continuous 450 W Xe lamp in the steady state mode or a Horiba Scientific NanoLed 300 (maximum at 303 nm) for fluorescence lifetime measurements. Detection was performed with a Hamamatsu R928 photomultiplier and the emission spectra were corrected for instrumental response using correction functions furnished by the supplier. Fluorescence decays were fitted with the FAST program from Edinburgh Instruments. Fluorescence quantum yields were determined on optically diluted solutions (o.d. < 0.05) using tryptophan (Sigma, 98%) at pH = 7.2 in HEPES buffer as the reference ($\phi_{\text{ref}} = 0.14$).[65] The fluorescence quantum yields, ϕ, were obtained with the relation:

$$\phi = \phi_{\text{ref}} \times \left(\frac{\text{o.d.}_{\text{ref}}}{\text{o.d.}} \right) \times \left(\frac{n}{n_{\text{ref}}} \right)^2 \times \left(\frac{\int I_{\text{em}}(\lambda)\mathrm{d}\lambda}{\int I_{\text{emref}}(\lambda)\mathrm{d}\lambda} \right)$$

in which o.d. stands for the optical density at the excitation wavelength, n is the refractive index of the medium, and $I_{\text{em}}(\lambda)$ is the emitted intensity at the wavelength λ.[14]

Computational details. Full geometry optimizations of the $[\textbf{ML1}]^{2+}$, $[\textbf{ML2}]^{2+}$ and $[\textbf{ML3}]^{2+}$ complexes (M = Hg or Cu) were performed in acetonitrile solution employing DFT calculations within the hybrid meta-GGA approximation with the TPSSh exchange–correlation functional[66] and the Gaussian 09 package (Revision D.01).[67] For the Hg^{2+} complexes the standard Ahlrichs' valence triple-ξ including polarization functions (TZVP)[68] basis set was used for all atoms except Hg, which was described using the relativistic effective core potential of Figgen *et al.* (ECP60MDF) and its associated (12s12p9d3f2g)/[6s6p4d3f2g] valence basis set.[69] For the cupric complexes Ahlrichs' split-valence polarized basis set (SVP) was used throughout.[70] Solvent effects were included by using the polarizable continuum model (PCM), in which the solute cavity is built as an envelope of spheres centered on atoms or atomic groups with appropriate radii. In particular, we used the integral equation formalism (IEFPCM) variant as implemented in Gaussian 09.[71] No symmetry constraints have been imposed during the optimizations. The stationary points found on the potential energy surfaces as a result of geometry optimizations were tested to represent energy minima rather than saddle points *via* frequency analysis. Time-dependent density functional theory (TDDFT)[72] was used for the calculation of the 40 lowest energy singlet–singlet electronic transitions of $[\textbf{HgL2}]^{2+}$ in acetonitrile solution.

X-ray crystallography. The crystals were placed in an oil, and a single crystal was selected, mounted on a glass fibre and placed in a low-temperature N$_2$ stream. For ligand **L2**, X-ray diffraction data collection was

carried out on a Nonius Kappa-CCD diffractometer equipped with an Oxford Cryosystem liquid N_2 device, using Mo-Kα radiation ($\lambda = 0.71073$ Å). The crystal–detector distance was 36 mm. The cell parameters were determined (Denzo software)[73] from reflections taken from one set of 10 frames (1.0° steps in phi angle), each at 20 s exposure. The structure was solved by direct methods using the program SHELXS-2013.[74] The refinement and all further calculations were carried out using SHELXL-2013.[75] The H-atoms were included in the calculated positions and treated as riding atoms using SHELXL default parameters. The non-H atoms were refined anisotropically, using weighted full-matrix least-squares on F^2.

For compound **1**, X-ray diffraction data collection was carried out on a Bruker APEX II DUO Kappa-CCD diffractometer equipped with an Oxford Cryosystem liquid N_2 device, using Mo-Kα radiation ($\lambda = 0.71073$ Å). The crystal–detector distance was 38 mm. The cell parameters were determined (APEX2 software)[76] from reflections taken from three sets of 12 frames, each at 10 s exposure. The structure was solved by direct methods using the program SHELXS-2013.[74] The refinement and all further calculations were carried out using SHELXL-2013.[75] The H-atoms were included in the calculated positions and treated as riding atoms using SHELXL default parameters. The non-H atoms were refined anisotropically, using weighted full-matrix least-squares on F^2. A semi-empirical absorption correction was applied using SADABS in APEX2;[76] transmission factors: $T_{min}/T_{max} = 0.6977/0.7456$. The SQUEEZE instruction in PLATON[77] was applied.

Notes and references

1. (*a*) J. B. Niederl and H. J. Vogel, *J. Am. Chem. Soc.*, 1940, **62**, 2512; (*b*) A. Zinke and E. Ziegler, *Ber.*, 1944, **77**, 264.

2. *Calixarenes 2001*, ed. Z. Asfari, V. Böhmer, J. Harrowfield and J. Vicens, Kluwer Academic Publishers, Dordrecht, The Netherlands, 2001.

3. A. F. Danil de Namor, R. M. Cleverly and M. L. Zapata-Ormachea, *Chem. Rev.*, 1998, **98**, 2495.

4. V. Lamare, J. F. Dozol, S. Fuangswasdi, F. Arnaud-Neu, P. Thuery, M. Nierlich, Z. Asfari and J. Vicens, *J. Chem. Soc., Perkin Trans. 2*, 1999, 271.

5. See for examples: (*a*) K. M. H. Wang, Y. M. Qi, S.-Y. Liu, T. C. Lee, W. Choy and J. Chen, *US patent*WO1994003165A1, 1994; (*b*) T. Ghosh, *Patent*EP954965, 1999 (C.A. 131:318951z).

6. (*a*) L. Prodi, S. Pivari, F. Boletta, M. Hissler and R. Ziessel, *Eur. J. Inorg. Chem.*, 1998, 1959; (*b*) F. d. M. Ramirez, L. Charbonnière, G. Muller and J.-C. G. Bünzli, *Eur. J. Inorg. Chem.*, 2004, 2348.

7. F. Sansone, S. Barboso, A. Casnati, D. Sciotto and R. Ungaro, *Tetrahedron Lett.*, 1999, **40**, 4741.

8. J.-P. Scharff and M. Mahjoubi, *New J. Chem.*, 1987, 2297.

9. (*a*) A. Casnati, R. Ungaro, Z. Asfari and J. Vicens, in *Calixarenes 2001*, ed. Z. Asfari, V. Böhmer, J. Harrowfield and J. Vicens, Kluwer Acadamic Publishers, Dordrecht, The Netherlands, 2001, p. 365; (*b*) V. Lamare, J. F. Dozol, P. Thuéry, M. Nierlich, Z. Asfari and J. Vicens, *J. Chem. Soc., Perkin Trans. 2*, 2001, 1920; (*c*) S. Bouhroum, F. Arnaud-Neu, Z. Asfari and J. Vicens, *Supramol. Chem.*, 2005, **17**, 629; (*d*) S. Bouhroum, F. Arnaud-Neu, Z. Asfari and J. Vicens, *Russ. Chem. Bull. Int. Ed.*, 2004, **53**, 1544; (*e*) M. W. Hosseini, in *Calixarenes 2001*, ed. Z. Asfari, V. Böhmer, J. Harrowfield and J. Vicens, Kluwer Acadamic Publishers, Dordrecht, The Netherlands, 2001, p. 110.

10. S. Bouhroum, J. S. Kim, S. W. Lee, P. Thuéry, G. Yap, F. Arnaud-Neu and J. Vicens, *J. Inclusion Phenom. Macrocyclic Chem.*, 2008, **62**, 239.

11. V. Csokai, A. Grün, B. Balazs, A. Simon, G. Toth and I. Bitter, *Tetrahedron*, 2006, **62**, 10215.

12. V. V. Khrizanforova, I. R. Knyazeva, I. R. Nizamiev, T. V. Gryaznova, V. I. Sokolova, S. A. Krasnov, M. K. Kadirov, A. R. Burilov, Yu. G. Budnikova and O. G. Sinyashin, *Russ. J. Gen. Chem.*, 2013, **83**, 663.

13. E. Makrlik, P. Vanura, P. Selucky and Z. Asfari, *J. Inclusion Phenom. Macrocyclic Chem.*, 2015, **81**, 169.

14. See for examples: (*a*) I. Leray and B. Valeur, *Eur. J. Inorg. Chem.*, 2009, 3525; (*b*) J. S. Kim and D. T. Quang,*Chem. Rev.*, 2007, **107**, 3780; (*c*) R. Joseph, J. Prakash Chinta and C. P. Rao, *Inorg. Chem.*, 2011, **50**, 7050.

15. H. H. Fan, K. F. Li, X. L. Zhang, W. Yang, M. S. Wng and K. W. Cheah, *Chem. Commun.*, 2011, **47**, 3879.

16. J. Isaad and A. El Achari, *Tetrahedron*, 2013, **69**, 4866.

17. (*a*) T. Zhang, G. She, X. Qi and L. Mua, *Tetrahedron*, 2013, **69**, 7102; (*b*) G. Lin, H. Xu, Y. Cui, Z. Wang, Y. Yang and G. Qian, *Mater. Chem. Phys.*, 2013, **141**, 591.

18. M. Duta, Z. Asfari, N. Kruchinina, P. Thuéry, A. Hagège and M. Leroy, *Supramol. Chem.*, 2005, **17**, 221.

19. T. Takimoto, H. Tsue, H. Takahashi, R. Tamura and H. Sasaki, *Heterocyles*, 2014, **88**, 911.

20. (*a*) J. Y. Lee, H. J. Kim, C. S. Park, W. Sim and S. S. Lee, *Chem. – Eur. J.*, 2009, **15**, 8989; (*b*) W.-B. Sim, J.-Y. Lee, J.-C. Kwon, M.-J. Kim and J.-S. Kim, *Bull. Korean Chem. Soc.*, 2002, **23**, 879.

21. M. Perrin and D. Oehler, in *Calixarenes, a versatile class of macrocyclic compounds*, ed. J. Vicens and V. Böhmer, Kluwer Acadamic Publishers, Dordrecht, The Netherlands, 1991.

22. (*a*) M. A. Mc Kervey, E. M. Seward, G. Ferguson and B. L. Ruhl, *J. Org. Chem.*, 1986, **51**, 3581; (*b*) F. D. M. Ramirez, L. J. Charbonnière, G. Muller, R. Scopelliti and J.-C. G. Bünzli, *Dalton Trans.*, 2001, 3205.

23. B. Valeur, in *Molecular Fluorescence*, Wiley-VCH, Weinheim, Germany, 2002.

24. (*a*) H. Kämmerer and G. Happel, *Monatsh. Chem.*, 1981, **112**, 759; (*b*) L. J. Charbonnière, C. Balsiger, K. J. Schenk and J.-C. G. Bünzli, *J. Chem. Soc., Dalton Trans.*, 1998, 505–510.

25. F. A. Cotton and G. Wilkinson, in *Advanced inorganic chemistry – A comprehensive text*, John Wiley & sons, New York, 5th edn, 1988.

26. K. B. Yatsimirsii and V. V. Pavlishchuk, *J. Coord. Chem.*, 1996, **37**, 341.

27. H. Gampp, M. Maeder, C. J. Meyer and A. D. Zuberbühler, *Talanta*, 1985, **32**, 95.

28. H. Gampp, M. Maeder, C. J. Meyer and A. D. Zuberbühler, *Talanta*, 1985, **32**, 257.

29. H. Gampp, M. Maeder, C. J. Meyer and A. D. Zuberbühler, *Talanta*, 1986, **33**, 943.

30. P. G. Sennikov, A. A. Tumanov and A. N. Egorochkin, *J. Organomet. Chem.*, 1983, **248**, 17.

31. L. A. Cunningham, J. Li and Y. Lu, *J. Am. Chem. Soc.*, 1998, **120**, 4518.

32. (*a*) R. Tamilarasan and D. R. McMillin, *Inorg. Chem.*, 1986, **25**, 2037; (*b*) M. T. Hay, R. M. Milberg and Y. Lu, *J. Am. Chem. Soc.*, 1996, **118**, 11976.

33. (*a*) L. M. Utschig, J. W. Bryson and T. V. O'halloran, *Science*, 1995, **268**, 380 ; (*b*) L. M. Utschig, J. G. Wright, G. Dieckmann, V. Pecoraro and T. V. O'halloran, *Inorg. Chem.*, 1995, **34**, 2497; (*c*) M. Vasak, J. H. R. Kaegi and H. A. O. Hill, *Biochemistry*, 1981, **20**, 2852; (*d*) L. M. Utschig, J. G. Wright and T. V. O'Halloran,*Methods Enzymol.*, 1993, **226**, 71.

34. S. P. Watton, J. G. Wright, F. M. MacDonnell, J. W. Bryson, M. Sabat and T. V. O'Halloran, *J. Am. Chem. Soc.*, 1990, **112**, 2824.

35. R. G. Pearson, *J. Chem. Educ.*, 1968, **45**, 581.

36. (*a*) V. V. Pavlishchuk and A. W. Addison, *Inorg. Chim. Acta*, 1993, **203**, 29; (*b*) B. Adhikary and R. Lucas, *Inorg. Chem.*, 1994, **33**, 1376.

37. J. G. Gilbert, A. W. Addison, A. Y. Nazarenko and R. J. Butcher, *Inorg. Chim. Acta*, 2001, **324**, 123.

38. E. L. Solomon, K. W. Penfield and D. E. Wilcox, *Struct. Bonding*, 1983, **53**, 1.

39. F. Hasanvand, A. Hoseinzadeh, J. Zolgharnein and S. Amani, *J. Coord. Chem.*, 2010, **63**, 346.

40. B. Turner and S. Swavey, *Inorg. Chem. Commun.*, 2007, **10**, 209.

41. S. Torelli, C. Belle, I. Gautier-Luneau, J. L. Pierre, E. Saint-Aman, J. M. Latour, L. Le Pape and D. Luneau, *Inorg. Chem.*, 2000,**39**, 3526.

42. (*a*) W. Sliwa and M. Deska, *ARKIVOC*, 2008, 87; (*b*) R. Ziessel, L. J. Charbonnière, M. Cesario, T. Prangé, M. Guardigli, A. Van Dorsselaer and H. Nierengarten, *Supramol. Chem.*, 2003, **15**, 277.

43. B. Mokhtari, K. Pourabdollah and N. Dalali, *J. Coord. Chem.*, 2011, **64**, 743.

44. R. Joseph and C. P. Rao, *Chem. Rev.*, 2011, **111**, 4658.

45. R. K. Pathak, V. K. Hinge, K. Mahesh, A. Rai, D. Panda and C. P. Rao, *Anal. Chem.*, 2012, **84**, 6907.

46. (*a*) R. K. Pathak, K. Tabbasum, A. Rai, D. Panda and C. P. Rao, *Analyst*, 2012, **137**, 4069–4075; (*b*) R. K. Pathak, K. Tabbasum, A. Rai, D. Panda and C. P. Rao, *Anal. Chem.*, 2012, **84**, 5117.

47. (*a*) R. K. Pathak, V. K. Hinge, M. Mondal and C. P. Rao, *J. Org. Chem.*, 2011, **76**, 10039; (*b*) R. K. Pathak, V. K. Hinge, A. Rai, D. Panda and C. P. Rao, *Inorg. Chem.*, 2012, **51**, 4994; (*c*) R. K. Pathak, A. G. Dikundwar, T. N. Guru Row and C. P. Rao, *Chem. Commun.*, 2010, **46**, 4345.

48. R. K. Pathak, K. Tabbasum, V. K. Hinge and C. P. Rao, *Chem. – Eur. J.*, 2011, **17**, 13999.

49. (*a*) R. Joseph, J. P. Chinta and C. P. Rao, *J. Org. Chem.*, 2010, **75**, 3387; (*b*) R. K. Pathak, S. M. Ibrahim and C. P. Rao, *Tetrahedron Lett.*, 2009, **50**, 2730.

50. (*a*) R. Joseph, B. Ramanujam, A. Acharya, A. Khutia and C. P. Rao, *J. Org. Chem.*, 2008, **73**, 5745; (*b*) J. Dessingou, K. Tabbasum, A. Mitra, V. K. Hinge and C. P. Rao, *J. Org. Chem.*, 2012, **77**, 1406.

51. A. Bandela, J. Prakash Chinta and C. P. Rao, *Dalton Trans.*, 2011, **40**, 11367.

52. A. Melchior, E. Peralta, M. Valiente and M. Tolazzi, *Polyhedron*, 2014, **75**, 88.

53. A. Melchior, E. Peralta, M. Valiente, C. Tavagnacco, F. Endrizzi and M. Tolazzi, *Dalton Trans.*, 2013, **42**, 6074.

54. (*a*) M. L. Helm, G. P. Helton, D. G. VanDerveer and G. J. Grant, *Inorg. Chem.*, 2005, **44**, 5696; (*b*) M. Wilhelm, S. Deeken, E. Berssen, W. Saak, A. Lützen, R. Koch and H. Strasdeit, *Eur. J. Inorg. Chem.*, 2004, 2301; (*c*) A. J. Blake, A. J. Holder, T. I. Hyde, G. Reid and M. Schröder, *Polyhedron*, 1989, **8**, 2041; (*d*) A. J. Blake, W.-S. Li, V. Lippolis, A. Taylor and M. Schröder, *J. Chem. Soc., Dalton Trans.*, 1998, 2931.

55. B. J. Hathaway, *Struct. Bonding*, 1984, **57**, 55.

56. B. J. Hathaway and D. E. Billing, *Coord. Chem. Rev.*, 1970, **5**, 143.

57. G. L. Miessler and D. A. Tarr, *Inorganic Chemistry*, Pearson Prentice Hall, 3rd edn, 2004.

58. B. J. Hathaway, M. Duggan, A. Murphy, J. Mullane, C. Power, A. Walsh and B. Walsh, *Coord. Chem. Rev.*, 1981, **36**, 267.

59. H. Irving and R. J. P. Williams, *J. Chem. Soc.*, 1953, 3192.

60. C. D. Gutsche, J. A. Levine and P. K. Sujeeth, *J. Org. Chem.*, 1985, **50**, 5802.

61. H. E. Gottlieb, V. Kotlyar and A. Nudelman, *J. Org. Chem.*, 1997, **62**, 7512.

62. D. W. Marquardt, *J. Soc. Ind. Appl. Math.*, 1963, **11**, 431.

63. M. Maeder and A. D. Zuberbühler, *Anal. Chem.*, 1990, **62**, 2220.

64. L. Alderighi, P. Gans, A. Ienco, D. Peters, A. Sabatini and A. Vacca, *Coord. Chem. Rev.*, 1999, **184**, 311.

65. D. F. Eaton, *Pure Appl. Chem.*, 1988, **60**, 1107.

66. J. M. Tao, J. P. Perdew, V. N. Staroverov and G. E. Scuseria, *Phys. Rev. Lett.*, 2003, **91**, 146401.

67. M. J. Frisch, G. W. Trucks, H. B. Schlegel, G. E. Scuseria, M. A. Robb, J. R. Cheeseman, G. Scalmani, V. Barone, B. Mennucci, G. A. Petersson, H. Nakatsuji, M. Caricato, X. Li, H. P. Hratchian, A. F. Izmaylov, J. Bloino, G. Zheng, J. L. Sonnenberg, M. Hada, M. Ehara, K. Toyota, R. Fukuda, J. Hasegawa, M. Ishida, T. Nakajima, Y. Honda, O. Kitao, H. Nakai, T. Vreven, J. A. Montgomery Jr., J. E. Peralta, F. Ogliaro, M. Bearpark, J. J. Heyd, E. Brothers, K. N. Kudin, V. N. Staroverov, R. Kobayashi, J. Normand, K. Raghavachari, A. Rendell, J. C. Burant, S. S. Iyengar, J. Tomasi, M. Cossi, N. Rega, N. J. Millam, M. Klene, J. E. Knox, J. B. Cross, V. Bakken, C. Adamo, J. Jaramillo, R. Gomperts, R. E. Stratmann, O. Yazyev, A. J. Austin, R. Cammi, C. Pomelli, J. W.

Ochterski, R. L. Martin, K. Morokuma, V. G. Zakrzewski, G. A. Voth, P. Salvador, J. J. Dannenberg, S. Dapprich, A. D. Daniels, Ö. Farkas, J. B. Foresman, J. V. Ortiz, J. Cioslowski and D. J. Fox, *Gaussian 09, Revision D.01*, Gaussian, Inc., Wallingford CT, 2009.

68. A. Schaefer, C. Huber and R. Ahlrichs, *J. Chem. Phys.*, 1994, **100**, 5829.

69. D. Figgen, G. Rauhut, M. Dolg and H. Stoll, *Chem. Phys.*, 2005, **311**, 227.

70. A. Schaefer, H. Horn and R. Ahlrichs, *J. Chem. Phys.*, 1992, **97**, 2571.

71. J. Tomasi, B. Mennucci and R. Cammi, *Chem. Rev.*, 2005, **105**, 2999.

72. (*a*) R. E. Stratmann, G. E. Scuseria and M. J. Frisch, *J. Chem. Phys.*, 1998, **109**, 8218; (*b*) R. Bauernschmitt and R. Ahlrichs, *Chem. Phys. Lett.*, 1996, **256**, 454; (*c*) M. E. Casida, C. Jamorski, K. C. Casida and D. R. Salahub, *J. Chem. Phys.*, 1998, **108**, 4439.

73. *Kappa CCD Operation Manual*, ed. B. V. Nonius, Delft, The Netherlands, 1997.

74. G. M. Sheldrick, *Acta Crystallogr., Sect. A: Fundam. Crystallogr.*, 1990, **46**, 467.

75. G. M. Sheldrick, *Acta Crystallogr., Sect. A: Fundam. Crystallogr.*, 2008, **64**, 112.

76. *M86-E01078 APEX2 User Manual*, Bruker AXS Inc., Madison, USA, 2006.

77. A. L. Spek, *J. Appl. Crystallogr.*, 2003, **36**, 7.